Cell Reports

Article

Recognition of the inherently unstable H2A nucleosome by Swc2 is a major determinant for unidirectional H2A.Z exchange

Graphical abstract

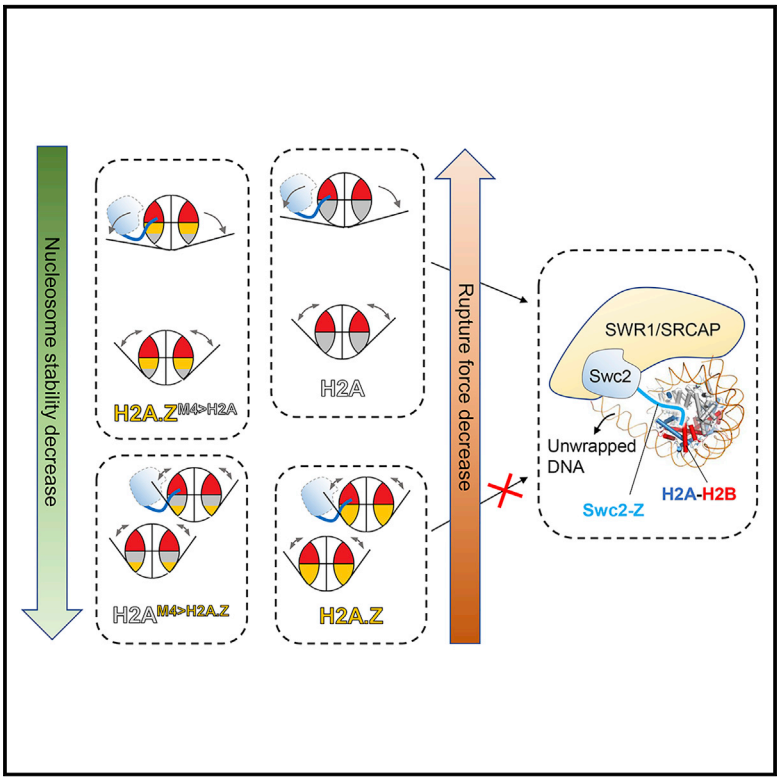

Highlights

- Swc2-Z is a specific Swc2 region interacting with the nucleosome acidic patch
- Swc2-Z facilitates the disassembly of the inherently unstable H2A nucleosome
- H2A and H2A.Z residues in M4 regions affect nucleosome stability
- Loss of Swc2-Z decreases SWR1 activity *in vitro* and *in vivo*

Authors

Linchang Dai, Xue Xiao, Lu Pan, ..., Bing Zhu, Wei Li, Zheng Zhou

Correspondence

weili007@iphy.ac.cn (W.L.), zhouzh@ibp.ac.cn (Z.Z.)

In brief

Dai et al. show that the H2A residues in the M4 region confer instability to the H2A nucleosome and further demonstrate that Swc2 specifically disassembles the unstable H2A nucleosome to ensure unidirectional H2A.Z exchange.

Dai et al., 2021, Cell Reports *35*, 109183
May 25, 2021
https://doi.org/10.1016/j.celrep.2021.109183

CellPress

Cell Reports

CellPress
OPEN ACCESS

Article

Recognition of the inherently unstable H2A nucleosome by Swc2 is a major determinant for unidirectional H2A.Z exchange

Linchang Dai,[1,6] Xue Xiao,[2,3,6] Lu Pan,[1] Liuxin Shi,[1,3] Ning Xu,[4] Zhuqiang Zhang,[1] Xiaoli Feng,[1] Lu Ma,[2] Shuoxing Dou,[2,3] Pengye Wang,[2,3,5] Bing Zhu,[1,3] Wei Li,[2,5,*] and Zheng Zhou[1,3,7,*]

[1]National Laboratory of Biomacromolecules, CAS Center for Excellence in Biomacromolecules, Institute of Biophysics, Chinese Academy of Sciences, Beijing 100101, China

[2]National Laboratory for Condensed Matter Physics and Key Laboratory of Soft Matter Physics, Institute of Physics, Chinese Academy of Sciences, Beijing 100190, China

[3]University of Chinese Academy of Sciences, Beijing 100049, China

[4]Beijing Advanced Innovation Center for Structural Biology, School of Life Sciences, Tsinghua University, Beijing 100084, China

[5]Songshan Lake Materials Laboratory, Dongguan, Guangdong 523808, China

[6]These authors contributed equally

[7]Lead contact

*Correspondence: weili007@iphy.ac.cn (W.L.), zhouzh@ibp.ac.cn (Z.Z.)

https://doi.org/10.1016/j.celrep.2021.109183

SUMMARY

The multisubunit chromatin remodeler SWR1/SRCAP/p400 replaces the nucleosomal H2A-H2B dimer with the free-form H2A.Z-H2B dimer, but the mechanism governing the unidirectional H2A-to-H2A.Z exchange remains elusive. Here, we perform single-molecule force spectroscopy to dissect the disassembly/reassembly processes of the H2A nucleosome and H2A.Z nucleosome. We find that the N-terminal 1–135 residues of yeast SWR1 complex protein 2 (previously termed Swc2-Z) facilitate the disassembly of nucleosomes containing H2A but not H2A.Z. The Swc2-mediated nucleosome disassembly/reassembly requires the inherently unstable H2A nucleosome, whose instability is conferred by three H2A α2-helical residues, Gly47, Pro49, and Ile63, as they selectively weaken the structural rigidity of the H2A-H2B dimer. It also requires Swc2-ZN (residues 1–37) that directly anchors to the H2A nucleosome and functions in the SWR1-catalyzed H2A.Z replacement *in vitro* and yeast H2A.Z deposition *in vivo*. Our findings provide mechanistic insights into how the SWR1 complex discriminates between the H2A nucleosome and H2A.Z nucleosome, establishing a simple paradigm for the governance of unidirectional H2A.Z exchange.

INTRODUCTION

Eukaryotic nuclear DNA is compacted into nucleosome core particles consisting of four histones, H2A, H2B, H3, and H4, and ~147-bp DNA (Luger et al., 1997). Canonical and variant H2A histones are essential players in regulating nucleosome properties and chromatin structures (Huang et al., 2020a). H2A.Z, a histone H2A variant required for yeast fitness and metazoan viability (Guillemette and Gaudreau, 2006), plays critical roles in gene transcription, DNA replication, DNA repair, and genome integrity maintenance (Henikoff and Smith, 2015; Venkatesh and Workman, 2015). The site-specific chromatin incorporation of H2A.Z is catalyzed by the remodeling complex SWR1 in budding yeast and SRCAP/p400 in human. Compared to remodeling complexes that can slide or disassemble the nucleosome, SWR1 mediates the unidirectional H2A-to-H2A.Z exchange by replacement of the nucleosomal H2A-H2B dimer (termed the A-B dimer) with the H2A.Z-H2B dimer (Z-B dimer) (Mizuguchi et al., 2004).

It has been shown that both the Z-B dimer and H2A nucleosome (A-Nuc) are required to activate SWR1 and initiate the histone replacement reaction (Luk et al., 2010; Wang et al., 2019). Specific recognition of the Z-B dimer is attributed to SWR1 subunits Swc2 and Swr1 (Wu et al., 2005, 2009), which directly interact with the H2A.Z αC helix (termed the M6 region) and L2 loop to fulfill their binding preference for H2A.Z (Hong et al., 2014; Latrick et al., 2016; Liang et al., 2016). The Swc2 N-terminal 1–135 residues, which preferentially recognize the Z-B dimer and govern H2A.Z incorporation, have been termed the Swc2-Z domain (Liang et al., 2016). Moreover, Swc2 is implicated in nucleosome-free region (NFR) binding (Yen et al., 2013) and SWR1 recruitment (Ranjan et al., 2013). Furthermore, Swc2 depletion causes the loss of unidirectional exchanges, indicating its regulatory role in determining the direction of H2A.Z exchange (Watanabe et al., 2013).

Despite recent advances in the study of Z-B dimer recognition, how SWR1 distinguishes the A-Nuc from the H2A.Z nucleosome (Z-Nuc) remains largely elusive. The cryoelectron microscopy (cryo-EM) structure of the SWR1-A-Nuc complex showed that the ATPase subunit of SWR1 distorts the nucleosomal DNA between SHL+2.5 and SHL+3.5, whereas the Swc6/Arp6 subunits

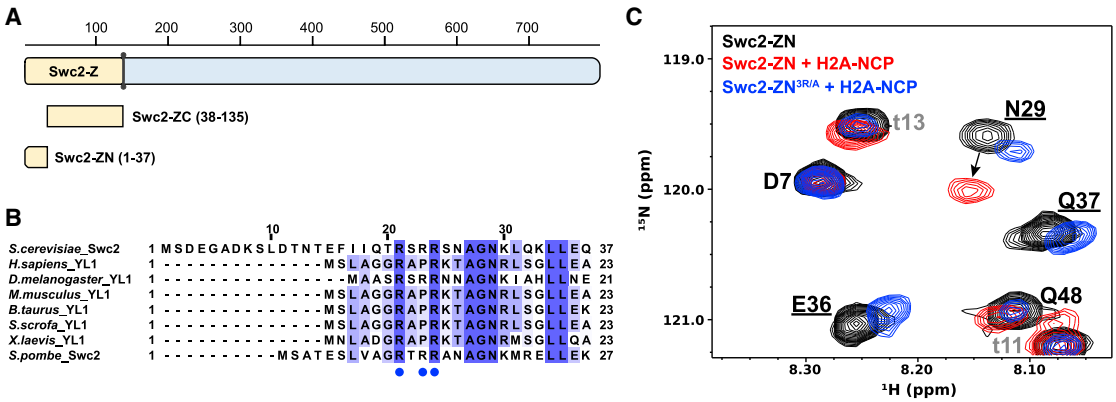

Figure 1. Swc2-ZN binds to the canonical nucleosome

(A) Schematic diagram of the Swc2 domain architecture. Swc2-Z, the Swc2 H2A.Z binding domain.

(B) Multiple-sequence alignment of the N-terminal region of Swc2/YL1 from different species. Blue dots indicate the conserved arginine residues in the RXXR motif.

(C) Overlay of the ^{15}N-^{1}H HSQC spectra of $Swc2_{1–50}$ (Swc2 residues 1–50) in the nucleosome-free form (black) and nucleosome-bound form (red). The ^{15}N-^{1}H HSQC spectra of the nucleosome-bound $Swc2_{1–50}$-containing R21A/R23A/R24A mutation ($Swc2\text{-}ZN^{3R/A}$) is colored in blue. Swc2 residues 17–35 displaying significant chemical shift changes are underlined in black. Residues in the C-terminal tag of $Swc2_{1–50}$ are labeled as t1–t17 in gray.

unwrap the DNA between SHL+4.5 and SHL+7 (Willhoft et al., 2018). The conformational changes likely weaken the interaction between the outgoing A-B dimer and SHL±3 DNA and SHL±4 DNA (Willhoft et al., 2018), leading to A-B dimer eviction being facilitated by the SWR1 subunit named Swc5 (Huang et al., 2020b). Furthermore, a recent study revealed that the α1 helix, α2 helix, and L2 loop of H2A are involved in A-Nuc recognition, given that the interchange of the N-terminal portion of the α2 helix (termed the M4 region) of H2A for H2A.Z dramatically reduces SWR1 activity and causes yeast lethality (Ranjan et al., 2015). However, the H2A M4 region residues are not exposed on the nucleosome surface and seemingly not involved in SWR1-nucleosome interaction. The mechanism underlying nucleosome selectivity remains unclear (Armeev et al., 2019; Ranjan et al., 2015).

Histone variants can directly modulate nucleosome structure and stability (Tachiwana et al., 2011; Zhou et al., 2021). The A-Nuc and Z-Nuc possess distinct dynamic properties despite their nearly identical structures (Chen et al., 2013; Kim et al., 2016; Suto et al., 2000). The biological relevance of the altered Z-Nuc dynamics is poorly understood because the effect of H2A.Z on nucleosome stability has been controversial (Abbott et al., 2001; Chen et al., 2013; Kim et al., 2016; Osakabe et al., 2018; Park et al., 2004; Rudnizky et al., 2016; Thambirajah et al., 2006; Zlatanova and Thakar, 2008). It remains largely unknown whether nucleosome dynamic properties contribute to A-Nuc recognition.

Here, we perform single-molecule magnetic tweezer experiments to characterize the disassembly and reassembly processes of A-Nuc and Z-Nuc. The nucleosomal DNA undergoes wrapping and unwrapping under variable tension. We demonstrate that Swc2-Z uses a specific region to interact with the nucleosome surface and facilitates the disassembly and reassembly of A-Nuc but not Z-Nuc. Structural and biochemical analyses show that the H2A M4 region acts as the key element that confers inherent instability to A-Nuc and ensures Swc2-mediated nucleosome disassembly and reassembly. Our findings uncover the molecular basis of how H2A confers nucleosome specificity and reveal a mechanism by which the SWR1 subunit Swc2 discriminates nucleosomes possessing distinct dynamic properties.

RESULTS

Swc2-Z directly interacts with the canonical nucleosome

Swc2-Z in budding yeast consists of an uncharacterized N-terminal region termed Swc2-ZN (residues 1–37) and a well-studied C-terminal portion termed Swc2-ZC (residues 38–135) (Figures 1A and 1B). Swc2-Z and its ortholog YL1-Z (dYL1-Z in *Drosophila*, hYL1-Z in human) can interact with the histone A-B dimer and Z-B dimer (Liang et al., 2016; Wu et al., 2005). YL1-ZC plays a central role in determining the binding preference for the Z-B dimer over the A-B dimer, whereas YL1-ZN has a subtle effect on binding choice (Liang et al., 2016). Nevertheless, YL1-ZN has been observed to bind to the Z-B dimer in the dYL1-H2A.Z-H2B complex (Liang et al., 2016). Superimposing the Z-B dimer on the dYL1-H2A.Z-H2B complex with its counterpart in the human A-Nuc (PDB: 2CV5) (Tsunaka et al., 2005) places $dYL1_{1–21}$ (corresponding to $Swc2_{18–37}$) onto the nucleosome surface with no steric clashes (Figure S1A). In particular, the dYL1 residues R5 and R8 and Swc2 residues R21 and R24 form a highly conserved RXXR motif (X refers to un-conserved residues) that anchors to the nucleosome surface (Figure S1A). We next performed the NMR chemical shift perturbation (CSP) approach to examine the potential interactions between Swc2-ZN and A-Nuc. In brief, we compared the two-dimensional (2D) ^{1}H-^{15}N HSQC (heteronuclear single quantum coherence spectroscopy) spectra of $Swc2_{1–50}$ (Swc2 residues 1–50) and monitored the chemical shift change of each peak during nucleosome titration (Figure S1B). The

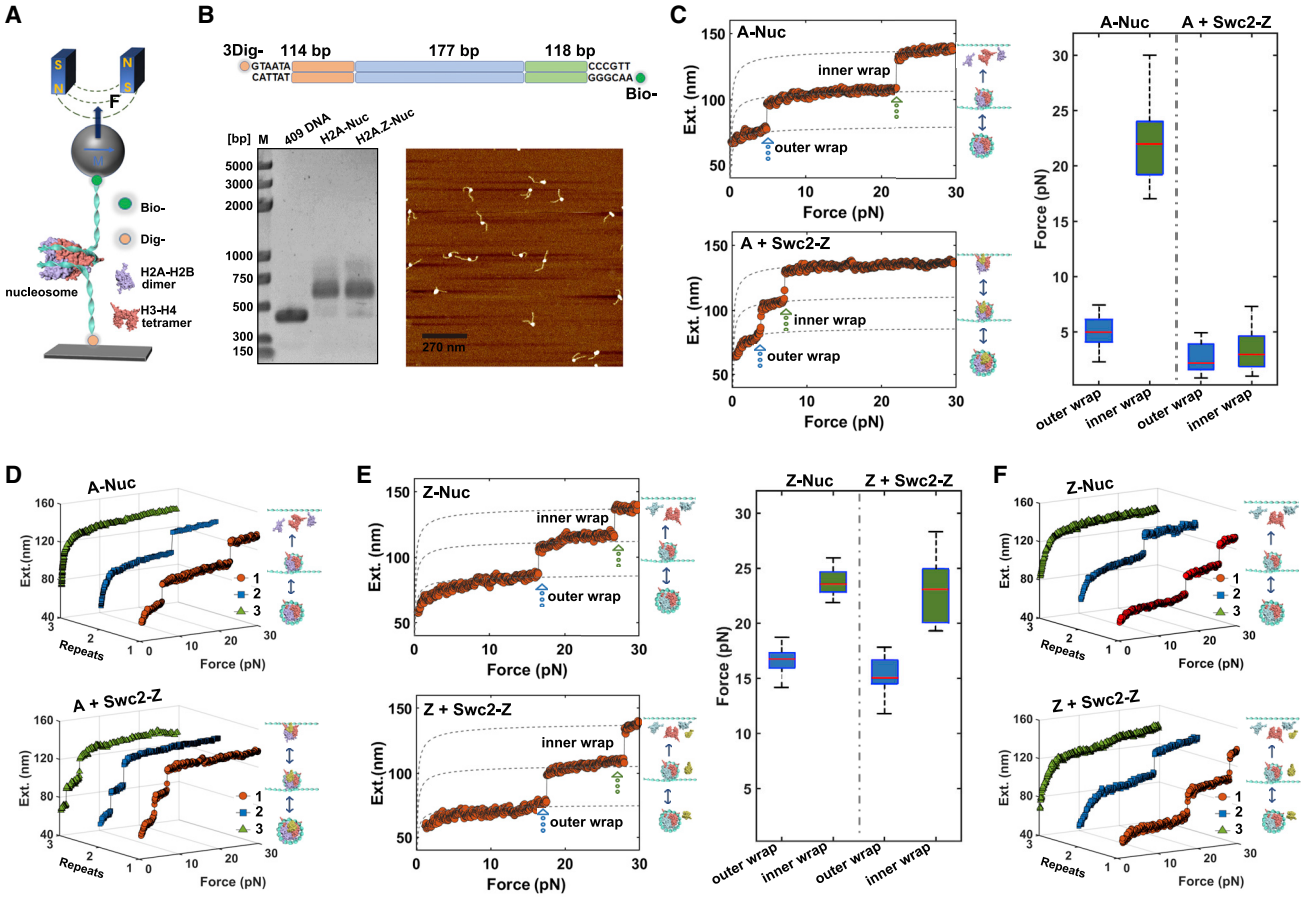

Figure 2. Swc2-Z preferentially disassembles the canonical nucleosome

(A) Schematic setup of the magnetic tweezers.

(B) AFM images and native gel electrophoresis of the nucleosome reconstituted on the DNA template shown at the top.

(C) Typical force-extension curves of the H2A nucleosome (A-Nuc) (top) without Swc2-Z and A-Nuc with Swc2-Z (bottom). The cartoons (right) represent the dynamics of the nucleosome without or with Swc2-Z. The dashed lines indicate three states of two-step unfolding force-extension curves fitted with 262-, 320-, and 409-bp free DNA, respectively, by the wormlike chain (WLC) model. Right: statistical rupture forces for the outer and inner DNA wraps for A-Nuc without Swc2-Z (left; n = 59) and A-Nuc with Swc2-Z (right; n = 47). Center lines show the median; box limits indicate the 1st and 3rd quartiles. n represents the number of data values.

(D) Repeated stretching measurements of a single A-Nuc without (top) and with (bottom) Swc2-Z, with the cartoons (right) representing the relative dynamic process of the nucleosome, respectively.

(E) Typical force-extension curves of the H2A.Z nucleosome (Z-Nuc) without Swc2-Z (top) and Z-Nuc with Swc2-Z (bottom). Right: statistical rupture forces for the outer and inner DNA wraps for Z-Nuc (left; n = 59) and Z-Nuc with Swc2-Z (right; n = 18). Center lines show the median; box limits indicate the 1st and 3rd quartiles. n represents the number of data values.

(F) Repeated stretching measurements of a single Z-Nuc without (top) and with (bottom) Swc2-Z.

CSPs are mostly mapped to Swc2$_{18–37}$, indicating the region of residues 18–37 is involved in nucleosome binding (Figure S1B). Typically, the resonances of Swc2-ZN residues are either remarkedly perturbed (Swc2 N29) or completely disappear (Swc2 E36 and Q37) upon nucleosome titration, whereas the resonances of Swc2 D7 and Q48 remain unchanged (Figure 1C). To verify the conclusion resulting from CSP analysis, we generate an Swc2-ZN$^{3R/A}$ mutant (R21A/R23A/R24A) to abolish the binding between the Swc2 RXXR motif and nucleosome surface. The resonances of Swc2-ZN$^{3R/A}$ N29, E36, and Q37 are unperturbed upon nucleosome titration, indicative of binding losses (Figures 1C, S1C, and S1D). These results strongly suggest that Swc2-ZN directly interacts with the nucleosome surface. Notably, this finding coincides with the structure of SWR1-nucleosome complexes in which an undefined Swc2 segment interacts with the nucleosome acidic patch (Willhoft et al., 2018).

Swc2-Z facilitates the disassembly of nucleosomes containing H2A but not H2A.Z

To assess the biological outcome of Swc2-ZN in recognizing nucleosomes, we investigated the influence of Swc2-Z on nucleosome assembly and disassembly using single-molecule magnetic tweezers (Figure 2A). The single-molecule magnetic tweezer approach can mimic nucleosome disassembly and

assembly processes and has been successfully employed to investigate nucleosome dynamics (Bintu et al., 2012; Chen et al., 2018). We reconstituted yeast A-Nuc or Z-Nuc by reconstituting both nucleosomes onto a 409-bp DNA fragment with a centered Widom 601 nucleosome-positioning sequence (Lowary and Widom, 1998) (Figure 2B). The native gel shift assay and atomic force microscopy (AFM) imaging results demonstrated that the nucleosomes were well positioned on the Widom 601 sequence (Figure 2B). A single nucleosome is stretched under continuously increasing tension at a rate of 0.05 pN/s in the presence or absence of Swc2-Z peptide. The structural transition of the nucleosome is monitored accordingly.

Yeast A-Nuc disassembly in the Swc2-Z-free condition is a two-step process. The outer and inner wraps of DNA are disassembled at ~5 pN and ~22 pN (Figure 2C, left top panel), coinciding with previous results (Hall et al., 2009; Li et al., 2016; Mihardja et al., 2006). However, in the presence of Swc2-Z, the rupture forces for the outer wrap and inner wrap of DNA are dramatically decreased to ~2 pN and ~8 pN (Figure 2C, left bottom panel). Statistical characterization shows that Swc2-Z facilitates A-Nuc disassembly (Figure 2C, right panel). A two-step disassembly mode of A-Nuc is maintained in the repeated stretching cycles when Swc2-Z is present (Figure 2D, bottom panel). However, in the absence of Swc2-Z, A-Nuc cannot restore the intact nucleosome structure after nucleosome disassembly (Figure 2D, top panel). These results suggest that the histone components tend to dissociate from the nucleosomal DNA during A-Nuc disassembly, but Swc2-Z can maintain A-Nuc integrity and prevents A-Nuc from falling apart. We next examined the disassembly and reassembly of yeast Z-Nuc. Surprisingly, although yeast Z-Nuc disassembly requires larger rupture forces (~15 pN and ~25 pN), Swc2-Z poses a limited facilitating effect on Z-Nuc disassembly (Figure 2E, right panel) and fails to maintain the integrity of Z-Nuc during the stretching cycles (Figure 2F). These results reveal a dual function of Swc2-Z in promoting nucleosome disassembly and maintaining nucleosome integrity and demonstrate that Swc2-Z exclusively affects the canonical nucleosome (A-Nuc).

H2A M4 region ensures nucleosome instability and Swc2-Z specificity

Comparative analyses reveal that A-Nuc requires lower rupture forces (~5 pN and ~22 pN) than does Z-Nuc (~15 pN and ~25 pN) to disassemble the nucleosome (Figures 2C and 2E), suggesting A-Nuc is mechanically less stable than Z-Nuc. We predicted that the inherent instability of A-Nuc might be a major determinant for Swc2-mediated nucleosome disassembly. Conceivably, a particular H2A element should exist to confer such instability to A-Nuc.

To test this assumption, we interchanged the M4 and M6 regions between H2A and H2A.Z. We measured the forces required to disassemble the mutated nucleosome to explore whether these H2A elements confer A-Nuc instability (Figure 3A). The M4 and M6 regions were selected because they are critical for SWR1-catalyzed histone replacement. Whereas interchange of the H2A M4 region for H2A.Z completely inactivates the SWR1 complex (Ranjan et al., 2015), the H2A.Z M6 region is responsible for conferring a preference to the Z-B dimer (Hong et al., 2014; Liang et al., 2016; Mao et al., 2014; Obri et al., 2014). We generated M4 region substitution mutants for H2A (termed $A^{M4>Z}$) and H2A.Z (termed $Z^{M4>A}$) by interchanging H2A residues 47–63 with the corresponding H2A.Z residues 54–70. As shown in the single-molecule experiments, the stability of $A^{M4>Z}$-Nuc is dramatically increased (Figure 3A, left top panel). The $A^{M4>Z}$-Nuc rupture forces increase to the same level as Z-Nuc's (Figure 3A, right panel), whereas the rupture forces of $Z^{M4>A}$-Nuc decrease to a similar level as A-Nuc's (Figure 3A, left bottom panel and right panel). Moreover, we interchanged H2A residues 90–101 and H2A.Z residues 87–107, generating the M6 region substitution mutants for H2A (termed $A^{M6>Z}$) and H2A.Z (termed $Z^{M6>A}$). However, interchanging the M6 region of H2A for H2A.Z, or vice versa, only showed a mild effect on nucleosome stability (Figure 3A, middle panel and right panel). These results suggest that the H2A M4 region plays a central role in conferring nucleosome instability to A-Nuc.

Nucleosome instability conferred by the H2A M4 region prompted us to assess the effect of the M4 region on nucleosome disassembly and reassembly in the presence of Swc2-Z. Remarkably, tensions required to disassemble $A^{M6>Z}$-Nuc (~2 pN and ~5 pN) and $A^{M4>Z}$-Nuc (~15 pN and 23 pN) indicate that Swc2-Z facilitates the disassembly of $A^{M6>Z}$-Nuc but not $A^{M4>Z}$-Nuc (Figure 3B). Moreover, during the repeated stretching, Swc2-Z maintains nucleosome integrity and presents specificity to $A^{M6>Z}$-Nuc rather than $A^{M4>Z}$-Nuc (Figure 3C). In line with these results, Swc2-Z exclusively facilitates the nucleosome disassembly and reassembly of $Z^{M4>A}$-Nuc but not $Z^{M6>A}$-Nuc (Figures 3D and 3E). In line with these findings, a previous study showed that SWR1 activity is abolished by substitution of the H2A M4 region but not the H2A M6 region for their H2A.Z counterparts (Ranjan et al., 2015).

Together, these results demonstrated that Swc2-Z specifically targets the nucleosomes destabilized by the H2A M4 region to fulfill Swc2-Z's function in nucleosome disassembly/reassembly. Our findings implicate that the selective recognition of the H2A M4 region by Swc2-Z is involved in the activation of SWR1-dependent histone replacement.

Structural basis for conferring nucleosome instability by the H2A M4 region

To dissect how the H2A M4 region confers A-Nuc's inherent instability, we first performed a multiple-sequence alignment to compare the M4 region residues of H2A and H2A.Z (Figures 4A and S2). Among all five yeast H2A residues discriminated from their H2A.Z counterparts, three are conserved across all species (yeast H2A G47, P49, and I63, corresponding to yeast H2A.Z K53, A55, and V70) (Figures 4A and S2). In contrast, sequence divergence between yeast H2A V50 and A60 and yeast H2A.Z I56 and T67 is not observed in higher eukaryotes. Therefore, H2A residues G47, P49, and I63 likely play a pivotal role in conferring A-Nuc instability.

Structural comparisons show that the yeast A-B dimer (PDB: 4WNN) (Kemble et al., 2015) closely resembles the A-B dimer in human A-Nuc (PDB: 2CV5) (Tsunaka et al., 2005) and the Z-B dimer in human Z-Nuc (PDB: 1F66) (Suto et al., 2000), with the root-mean-square deviation (RMSD) equal to 0.42 Å and 0.44 Å, respectively. Consistently, the overall structures of the

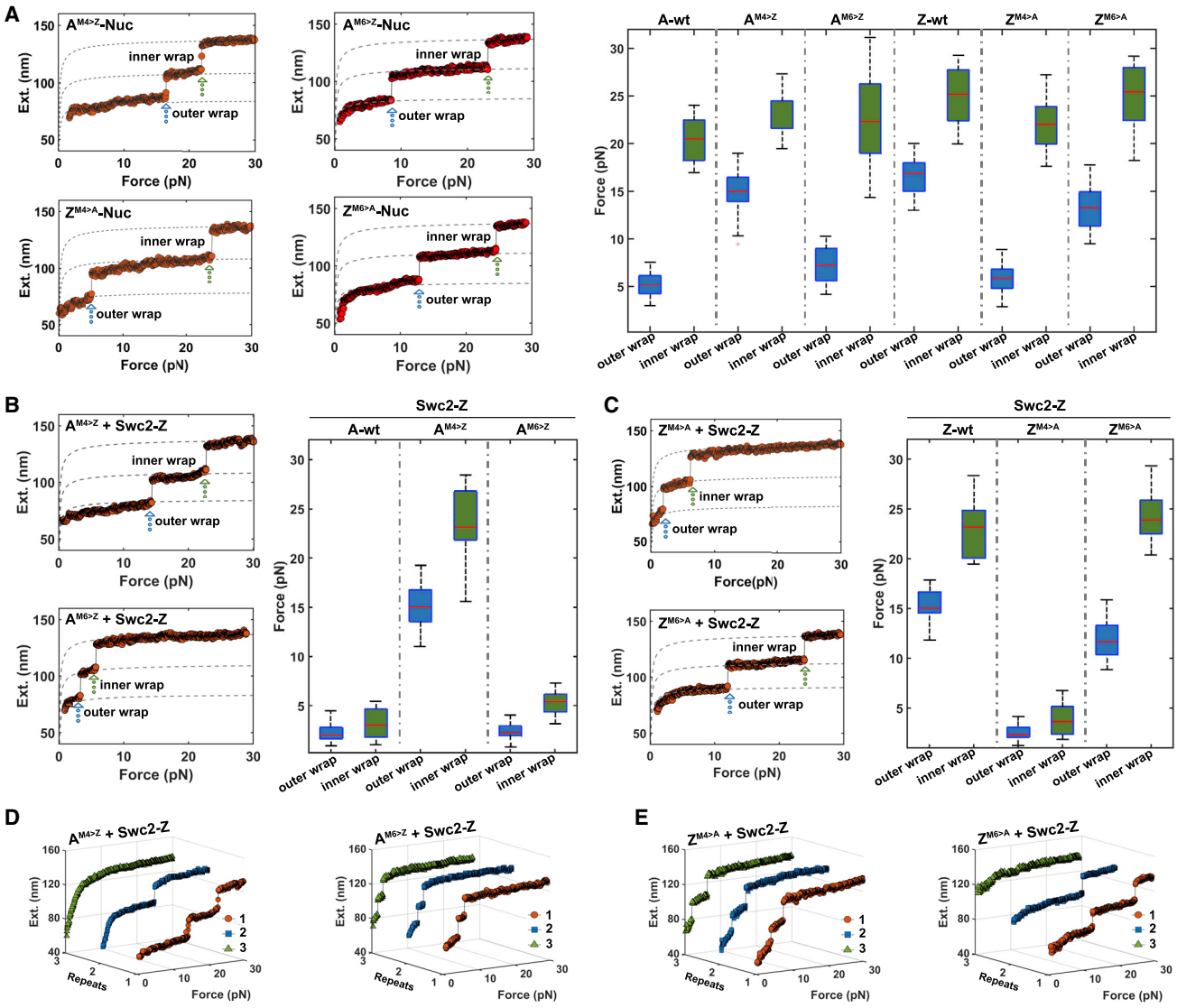

Figure 3. H2A M4 region is essential for Swc2-mediated nucleosome disassembly

(A) Typical force-extension curves of the H2A$^{M4>Z}$ nucleosome, H2A$^{M6>Z}$ nucleosome, H2A.Z$^{M4>A}$ nucleosome, and H2A.Z$^{M6>A}$ nucleosome (left and middle). Right: statistical rupture forces for the outer and inner DNA wraps for A-Nuc (n = 59), A$^{M4>Z}$ nucleosome (n = 38), A$^{M6>Z}$ nucleosome (n = 38), Z-Nuc (n = 59), Z$^{M4>A}$ nucleosome (n = 26), and Z$^{M6>A}$ nucleosome (n = 35), respectively. Center lines show the median; box limits indicate the 1st and 3rd quartiles. n represents the number of data values.

(B) Typical force-extension curves of the A$^{M4>Z}$ nucleosome with Swc2-Z (top) and A$^{M6>Z}$ nucleosome with Swc2-Z (bottom). Right: statistical rupture forces for the outer and inner DNA wraps for A-Nuc with Swc2-Z (left; n = 47), A$^{M4>Z}$ nucleosome with Swc2-Z (middle; n = 36), and A$^{M6>Z}$ nucleosome with Swc2-Z (right; n = 34). Center lines show the median; box limits indicate the 1st and 3rd quartiles. n represents the number of data values.

(C) Typical force-extension curves of the H2A.Z$^{M4>A}$ nucleosome with Swc2-Z (top) and H2A.Z$^{M6>A}$ nucleosome with Swc2-Z (bottom). Right: statistical rupture forces for the outer and inner DNA wraps for the Z-Nuc with Swc2-Z (left; n = 18), H2A.Z$^{M4>A}$ nucleosome with Swc2-Z (middle; n = 48), and H2A.Z$^{M6>A}$ nucleosome with Swc2-Z (right; n = 33). Center lines show the median; box limits indicate the 1st and 3rd quartiles. n represents the number of data values.

(D) Repeated stretching measurements of a single H2A$^{M4>Z}$ nucleosome with Swc2-Z (left) and a single H2A$^{M6>Z}$ nucleosome with Swc2-Z (right).

(E) Repeated stretching measurements of a single H2A.Z$^{M4>A}$ nucleosome with Swc2-Z (left) and a single H2A.Z$^{M6>A}$ nucleosome with Swc2-Z (right).

A-B dimer and Z-B dimer in the nucleosome-free form are similar (Dai et al., 2019). However, we suspected that these two dimers might have distinct local structures given that H2A and H2A.Z show 60% sequence similarity. To examine the H2A M4 region's effect on the A-B dimer structure, we generated a yeast A$^{Z>M4}$-B dimer by substituting the H2A M4 region for H2A.Z and determined the crystal structure of the yeast single-chain A$^{M4>Z}$-B dimer at 2.4-Å resolution (Figures 4B and 4C; Table S1).

Comparison of structures of the A-B dimer and A$^{M4>Z}$-B dimer eliminates the influence of H2A residues outside the M4 region.

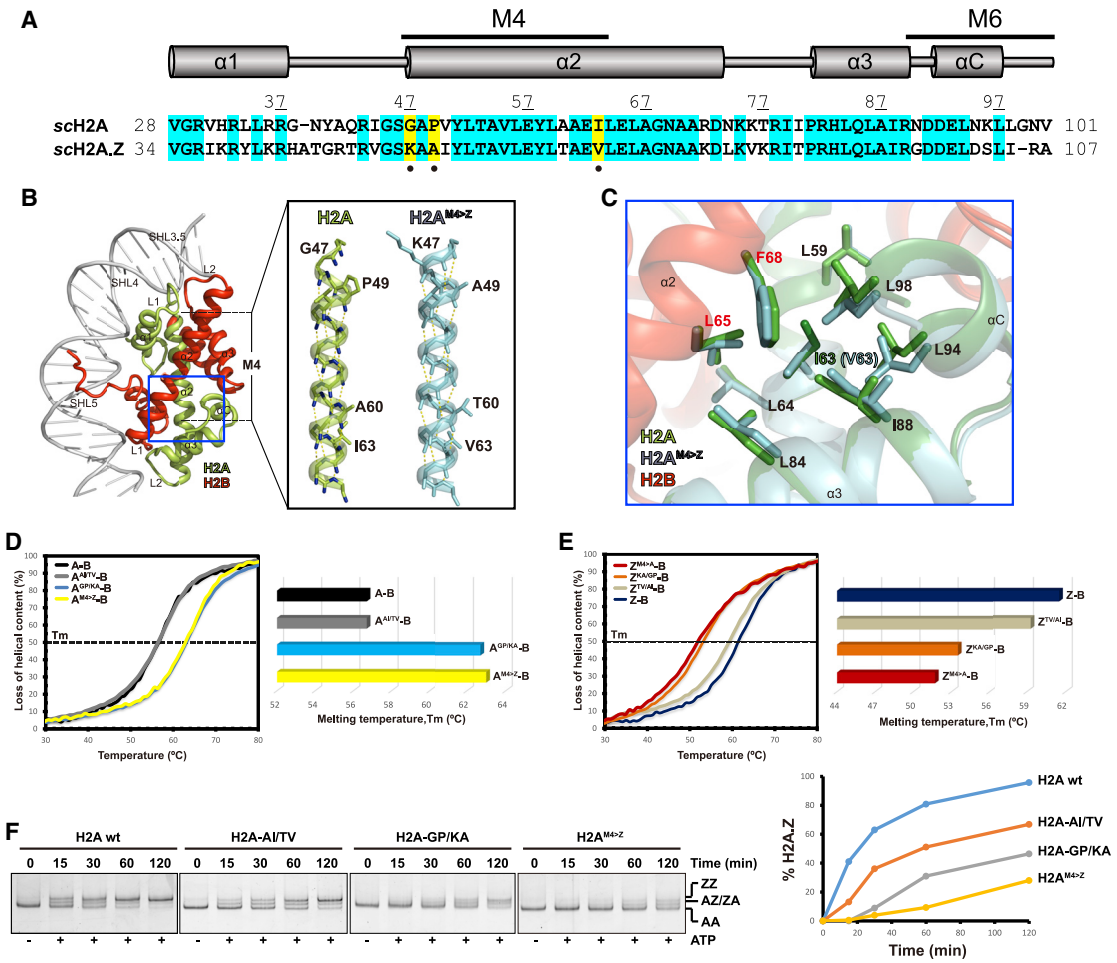

Figure 4. H2A Gly47, Pro49, and Ile63 confer inherent instability to the canonical nucleosome

(A) Sequence alignment of *Saccharomyces cerevisiae* histone H2A (*sc*H2A) and H2A.Z (*sc*H2A.Z). Secondary structures are indicated above the sequence. The M4 and M6 regions are highlighted with solid lines.

(B) Structural comparison of the A-B dimer (PDB: 4WNN) and nucleosomal A-B dimer (PDB: 2CV5). The A-B dimer and SHL3.5–SHL5.5 DNA are shown in cartoon representation (left). Highlighted in the rectangle are included the M4 regions of the A-B dimer (green) and $A^{M4>Z}$-B dimer (cyan) and the hydrogen bonds formed between the backbone carbonyl oxygen and amide nitrogen.

(C) Close-up view of H2A I63 in the A-B dimer (PDB: 4WNN) and V63 in the $A^{M4>Z}$-B dimer and hydrophobic residues surrounding these two residues. H2A, $H2A^{M4>Z}$, and H2B are colored in green, cyan, and red, respectively.

(D and E) Thermal denaturation of histone dimers.

(D) Melting curve of the A-B dimer and its mutants monitored by circular dichroism spectroscopy (left). Relative melting temperature (Tm) value of yeast H2A mutants as compared with the WT H2A (right).

(E) Melting curve of the Z-B dimer and its mutants (left). Relative Tm value of yeast H2A.Z mutants as compared with the WT H2A.Z (right).

(F) Native PAGE analysis to monitor histone exchange. SWR1 (2 nM) was mixed with 5 nM A-Nuc (or mutant) and 50 nM H2A.Z-$H2B^{FL}$ dimer for the indicated times at 23°C. The gel was scanned for SYBR green fluorescence (left). Right: H2A.Z incorporation curves.

The comparison reveals nearly identical structures for both dimers (RMSD equal to 0.285 Å) and several differences in the M4 regions of H2A and $H2A^{M4>Z}$. On the one hand, the α-helical region encompassing H2A residues G47–P49 shows fewer intrahelical hydrogen bonds than its counterpart residues K53–A55 in $H2A^{M4>Z}$, decreasing the structural rigidity of the H2A α2 helix (Figure 4B). It is conceivable that the P49 residue has no free NH group and cannot form backbone hydrogen bonds. Additionally, G47 and P49 tend to break α-helical structures, further reducing H2A α2-helical rigidity (Figure 4B). On the other hand, the hydrophobic residues surrounding I63 in H2A and V70 in $H2A^{M4>Z}$ undergo substantial side-chain rearrangement. The hydrophobic core repacking deforms the structure of cavities accommodating the H2A I63 and $H2A^{M4>Z}$ V70 (Figures 4C and S3). Therefore, the rigidity loss and contact change of the A-B dimer may alter the dynamic properties of A-Nuc. Compared to Z-Nuc, unstable A-Nuc could be more susceptible to Swc2-mediated nucleosome disassembly.

H2A M4 region alters histone dimer property and reduces SWR1 activity

The M4 region residues of H2A and H2A.Z confer distinct dynamic properties to A-Nuc and Z-Nuc that retain nearly identical overall structures. The striking results suggest an essential role of the local structural rigidity and contact mode, rather than the nucleosome structures, in distinguishing A-Nuc and Z-Nuc (Figure 4B). In light of these findings, we predict that the M4 region residues could affect yeast A-B and Z-B dimer properties by changing the local structural rigidity and contact mode. In light of these findings, we predict that the M4 region residues could affect yeast A-B and Z-B dimer properties by changing the local structural rigidity and contact mode, because the M4 region residues position in the histone dimer core region, which consist of the H2A (or H2A.Z) α2 helix and the H2B α2-α3 helices (Dai et al., 2019). To verify this assumption, we monitored the melting curve of the wild-type (WT) and mutated histone dimers by measuring the melting temperature (Tm) with circular dichroism (CD) spectroscopy (Figures 4D and 4E). Our results show that the H2A M4 region confers lower thermal stability to the histone dimer, as the Tm of the $Z^{M4>A}$-B dimer (52°C) is 10°C lower than the Tm of the Z-B dimer (62°C). In contrast, the A-B dimer (Tm 57°C) presents a 6°C lower Tm as compared to the $A^{M4>Z}$-B dimer (Tm 63°C) (Figures 4D and 4E). These results fully agree with our structural analyses and strongly implicate that the M4 region residues' rigidity and contact differences confer distinct dimer stabilities.

The M4 region residues are involved in binding between H2A and SHL3.5 DNA. To examine their effect on histone-DNA interaction, we performed an electrophoretic mobility shift assay (EMSA) to monitor histone-DNA complex formation during DNA titration (Figure S4A). In contrast to the $A^{M4>Z}$-B dimer, which possesses a higher DNA binding capability than the WT A-B dimer, the $Z^{M4>A}$-B dimer displays a lower DNA binding capability than the WT Z-B dimer (Figure S4B). The rigidity loss and contact change of the A-B dimer likely abrogate DNA-histone binding, albeit to a limited extent (Figure S4B). We next performed the SWR1-catalyzed histone H2A.Z replacement assay. We verified that the $H2A^{M4>Z}$ mutant causes a dramatic decrease in histone replacement (Figure 4F), a result coinciding with a previous finding (Ranjan et al., 2015).

Altogether, our findings suggest that the H2A M4 region causes the A-B dimer's rigidity losses and contact changes. The altered structure might decrease the thermostability and DNA binding of the A-B dimer and result in an unstable A-Nuc and defective H2A.Z exchange.

H2A G47 and P49 play a central role in histone replacement activation

Substitution of the H2A M4 region residues G47 and P49 for H2A.Z substantially reduces H2A.Z incorporation and yeast growth, indicating that residues in the H2A M4 region play a distinct role in A-Nuc destabilization (Ranjan et al., 2015). To further dissect the effect of M4 region residues, we interchanged H2A residues G47/P49 (or A60/I63) with their H2A.Z counterparts K53/A55 (or T67/V70) and measured the Tm of the histone dimers (Figures 4D and 4E). The H2A G47K/P49A mutation (corresponding to the $A^{GP/KA}$-B dimer) increases the Tm of the A-B dimer by 6°C, whereas the H2A.Z K53G/A55P mutation (corresponding to the $Z^{KA/GP}$-B dimer) decreases the Tm of the Z-B dimer by 8°C (Figures 4D and 4E). Conversely, the $A^{AI/TV}$-B dimer (or $Z^{TV/AI}$-B dimer) shows a similar Tm as compared to the A-B dimer (or Z-B dimer) (Figures 4D and 4E). These results suggested that H2A G47/P49 plays a central role in A-B dimer destabilization, whereas H2A A60/I63 has less effect on dimer stability.

Moreover, H2A G47/P49 exhibits a dramatic destabilization effect on the canonical nucleosome. The rupture forces for unwrapping the outer wrap of DNA are increased to ~14 pN for $A^{GP/KA}$-Nuc but decreased to 7 pN for $Z^{KA/GP}$-Nuc (Figures S5A and S5B). In contrast, the H2A A60T/I63V mutation slightly increases the rupture force required to open the outer-wrap DNA of the canonical nucleosome, whereas the DNA unwrapping of Z-Nuc is not changed by the H2A.Z T67A/V70I mutation (Figures S5C and S5D). Notably, the SWR1-catalyzed H2A.Z exchange is markedly impaired by $A^{GP/KA}$-Nuc but not by $Z^{TV/AI}$-Nuc containing the A60T/I63V mutation (Figure 4F). These results underscore the biological significance of H2A G47 and P49 in the chromatin incorporation of H2A.Z (Ranjan et al., 2015).

Altogether, we conclude that A-Nuc's inherent instability is mainly conferred by H2A M4 region residues G47 and P49, whereas H2A residues I63 and A60 are required for optimal SWR1 activity. These results suggest a rationale for the Swc2-dependent nucleosome recognition and unidirectional H2A.Z deposition.

An intact Swc2-Z is required for Swc2-mediated nucleosome disassembly

To elucidate the mechanism by which Swc2-Z facilitates the disassembly and reassembly of A-Nuc, we next asked whether Swc2-ZN alone can mediate the nucleosome disassembly and SWR1-dependent H2A.Z exchange. Strikingly, neither Swc2-ZN nor Swc2-ZC is sufficient to facilitate A-Nuc disassembly and reassembly, indicating they are both required for A-Nuc disassembly (Figure 5A, top panels). Consistently, the $Swc2\text{-}Z^{3R/A}$ mutant (R21A/R23A/R24A) and $H2A^{DEE/STT}$ mutant (D91S/E92T/E93T) failed to disassemble A-Nuc at the low tension, presumably due to their ability to disrupt the binding between Swc2-Z and the nucleosome surface (Figures 1C and 5A, bottom panels). Functional coordination between Swc2-ZN and Swc2-ZC suggests that the binding of Swc2-ZC and the A-B dimer is likely involved in the Swc2-mediated A-Nuc disassembly.

SRCAP/p400 subunit YL1 is the high-eukaryotic homolog of yeast Swc2 (Liang et al., 2016). We predicted that Swc2-dependent nucleosome disassembly might be conserved in high eukaryotes. To verify this assumption, we performed a single-molecule experiment using the human YL1-ZN (residues 4–23, termed hYL1-ZN) (Figure 1B). hYL1-Z reduced the human A-Nuc rupture force and facilitated the reassembly process of the human A-Nuc (Figure 5B). Importantly, hYL1-Z selectively disassembles human A-Nuc rather than human Z-Nuc, as does Swc2-Z in budding yeast (Figure 5B). We conclude that the mechanism of Swc2-dependent A-Nuc disassembly is conserved in all eukaryotes.

Loss of Swc2-ZN reduces H2A.Z incorporation *in vivo*

Swc2-Z has been demonstrated to be essential for SWR1 activity *in vitro* and H2A.Z incorporation *in vivo* (Liang et al., 2016). To exclude the influence of Swc2-ZC on SWR1 activity and H2A.Z

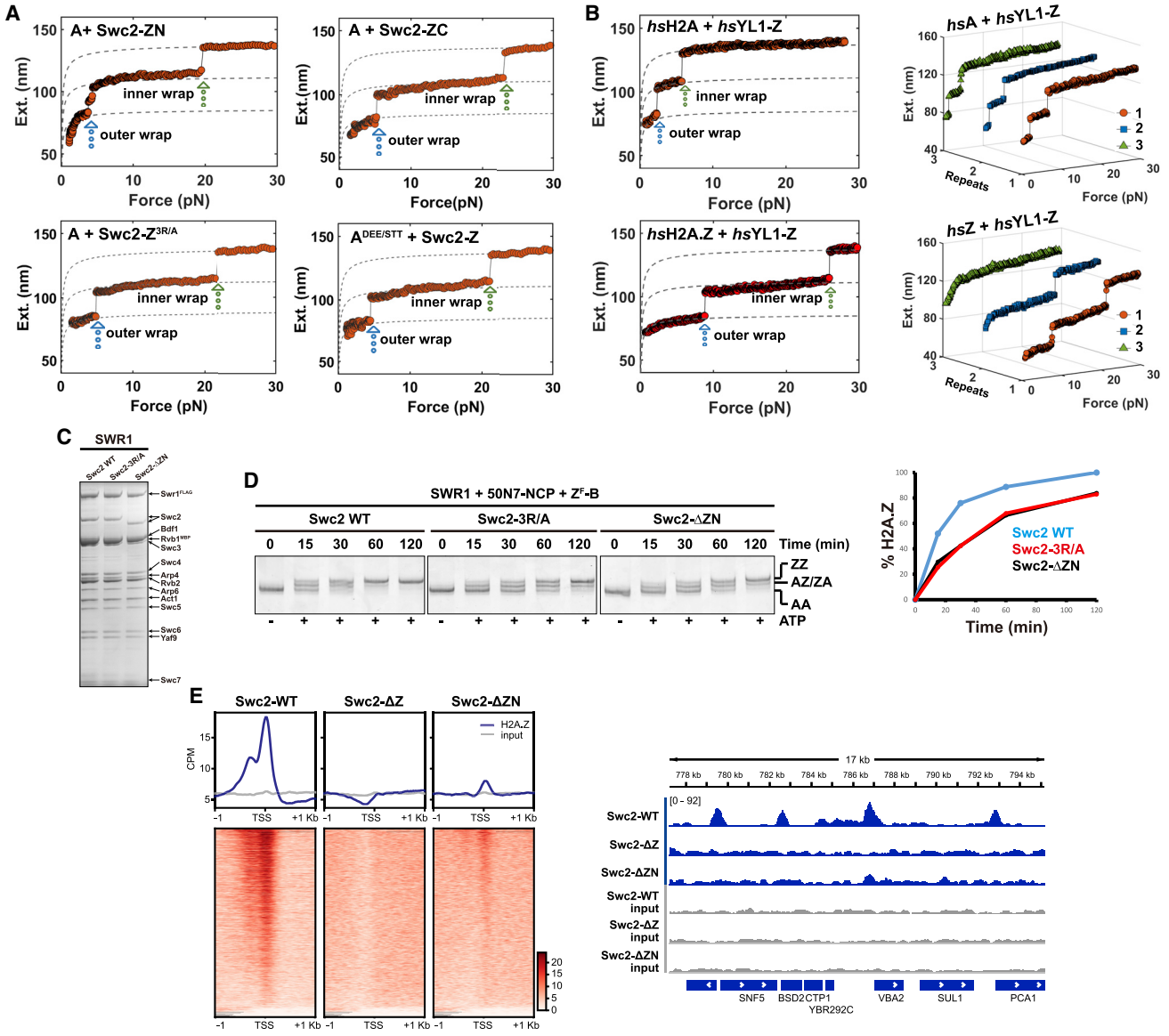

Figure 5. Swc2-ZN is essential for SWR1 activity and H2A.Z deposition

(A) Typical force-extension curves of A-Nuc with Swc2-ZN (top, left), A-Nuc with Swc2-ZC (top, right), A-Nuc with Swc2-$Z^{3R/A}$ (bottom, left), and $H2A^{DEE/STT}$ nucleosome with Swc2-Z (bottom, right).

(B) Typical force-extension curves of *hs*A-Nuc with *hs*YL1-Z (top, left) and *hs*Z-Nuc with *hs*YL1-Z (bottom, left). Repeated stretching measurements of a single *hs*A-Nuc with *hs*YL1-Z (top, right) and a single *hs*Z-Nuc with *hs*YL1-Z (bottom, right).

(C) SDS-PAGE showing subunit composition of SWR1 WT, SWR1 (Swc2-3R/A), and SWR1 (Swc2-ΔZN) complexes.

(D) Native PAGE analysis to monitor histone exchange. SWR1 (or mutants) (2 nM) was mixed with 5 nM A-Nuc and 50 nM H2A.Z-$H2B^{FL}$ for the indicated times at 16°C. The gel was scanned for SYBR green fluorescence (left). Right: H2A.Z incorporation curves.

(E) Heatmap showing H2A.Z occupancy around transcription start sites in Swc2 WT, Swc2-ΔZ, and Swc2-ΔZN yeast strains (left) and genome browser tracks of example genomic regions (right).

deposition, we generated Swc2-ΔZN (depletion of Swc2 1–37 residues) and Swc2-$Z^{3R/A}$ (R21A/R23A/R24A) mutants and examined how these two mutants affect the SWR1-mediated H2A.Z replacement *in vitro*. Compared to the full-length Swc2-Z (WT), both Swc2-ΔZN and Swc2-$Z^{3R/A}$ mutations decrease the SWR1 activity of the H2A.Z exchange (Figures 5C and 5D). These results suggest that Swc2-ZN is critical for the SWR1-mediated H2A.Z exchange.

To explore how Swc2-ZN affects H2A.Z deposition at the genome-wide level, we analyzed the budding yeast cells containing the full-length Swc2 (WT) or mutated Swc2 (Swc2-ΔZ and Swc2-ΔZN) using ChIP-seq (chromatin immunoprecipitation

sequencing) experiments (Figure 5E). All the genes were sorted according to their H2A.Z ChIP-seq reads at the transcription start site (TSS) regions. The H2A.Z occupancy profiles for all three yeast cells were compared. In the WT Swc2-Z cell, H2A.Z is enriched in +1 and −1 nucleosomes flanking the TSS regions (−300 bp to +300 bp) (Figure 5E). The H2A.Z occupancy at the +1 nucleosomes is significantly higher than that at the −1 nucleosomes, coinciding with previous findings (Luk et al., 2010). In the Swc2-ZN depletion cell (Swc2-ΔZN), H2A.Z occupancy at the +1 nucleosomes and the −1 nucleosomes is markedly decreased, indicating a global loss of H2A.Z occupancy at the TSS regions (Figure 5E). Strikingly, H2A.Z occupancy at the TSS is abolished when Swc2-Z is completely deleted (Swc2-ΔZ), underscoring the role of Swc2-ZC in H2A.Z incorporation (Figure 5E). These results are fully consistent with the aforementioned findings related to Swc2-ZC function.

Collectively, we conclude that Swc2-ZN is essential for SWR1-mediated H2A.Z replacement *in vitro* and deposition of budding yeast H2A.Z *in vivo*. Moreover, Swc2-ZN and Swc2-ZC are both required for H2A.Z incorporation.

DISCUSSION

We used the single-molecule magnetic tweezer approach to investigate how yeast SWR1 complex subunits recognize the canonical nucleosome to ensure unidirectional H2A.Z exchanges. We found that residues at the H2A M4 region induce the rigidity loss and contact change of the A-B dimer, thereby decreasing the breaking force for nucleosomes containing H2A but not H2A.Z. Importantly, SWR1 subunit protein 2 (Swc2) discriminates between A-Nuc and Z-Nuc by selectively disassembling the A-Nuc. Our study reveals the key elements in Swc2 (Swc2-Z) and in A-Nuc (M4 region) that serve as the major determinants of the unidirectional histone displacement. This work provides molecular insight into the nucleosome specificity conferred by histone H2A variant and chromatin remodeling complex subunits.

Single-molecule magnetic tweezers generate the DNA unwrapping involving the entry and exit DNA locations, mimicking the nucleosome assembly and disassembly processes. Notably, DNA unwrapping during SWR1-catalyzed histone replacement should be spatially limited between the location of the DNA translocation lobes and a counter-grip. The cryo-EM structure of the SWR1-nucleosome complex shows that the ATPase motor of SWR1 engages the tracking strand of SHL+2 DNA, whereas Swc6/Arp6 subunits unwrap 2.5 turns of DNA from the entry site and promote the distortion of SHL+2.5 and SHL+3.5 DNA (Willhoft et al., 2018). SWR1 may create a constrained bulge involving several ruptured histone-DNA contacts, whereas most other remodelers are involved in the propagation of a twist defect/translocation in the 1- to 3-bp range (Sun et al., 2020). Swc2 facilitates A-Nuc disassembly, indicating its ability to overcome the energy barrier that impedes ATPase-driven nucleosomal DNA unwrapping. Nonetheless, Swc2-Z needs to interact with A-Nuc and the Z-B dimer to fulfill its function, coinciding with the SWR1-nucleosome complex structure showing that an Swc2 segment interacts with the nucleosome acidic patch (Willhoft et al., 2018).

In contrast to Swc2-ZN, the interaction between Swc2-ZC and the Z-B dimer is indispensable for preferential recognition of the Z-B dimer. However, the sequence similarity of Swc2-ZN is not low as compared to Swc2-ZC, indicating that the function of this uncharacterized portion of Swc2 is rather critical (Figure 1C). One clue to support this prediction is that Swc2-ZN indeed interacts with the nucleosome surface (Figures 1C and S1). This interaction has been observed in the dYL1-H2A.Z-H2B complex structure (Liang et al., 2016). It fits well with the SWR1-nucleosome complex structure that displays a presumed Swc2-nucleosome interaction (Willhoft et al., 2018). A second clue is that depletion of Swc2-ZN inactivates the SWR1-catalyzed histone replacement *in vitro* and reduces the H2A.Z incorporation *in vivo* (Figure 4). Furthermore, we demonstrate that the Swc2-Z homolog in human SRCAP complex subunit YL1 displays similar selectivity to the human A-Nuc, suggesting that a conserved mechanism for Swc2/YL1-mediated A-Nuc recognition is repeatedly used in all eukaryotes (Figure 1C). These findings provide a rationale for identifying canonical nucleosomes by SWR1 subunit proteins and thus relate nucleosome dynamic properties to unidirectional histone displacement.

The M4 region residues of both H2A and H2A.Z are embedded within the nucleosome, whereby they are less exposed and inaccessible for SWR1 recognition. This work demonstrates that H2A M4 region residues confer inherent instability to A-Nuc (Figure 3A). Compared to the H2A.Z counterparts, H2A M4 region residues G47/P49 are prone to disrupt backbone hydrogen bonds and break the α-helical formation, whereas H2A residue I63 tends to induce hydrophobic core repacking. The structural rigidity losses and contact changes decrease the thermostability of the A-B dimer and A-Nuc, facilitating the nucleosome disassembly of A-Nuc (Figures 3A, 4D, and 4E). The structural elasticity likely reduces the interaction between the A-B dimer and SHL3.5 DNA, leading to DNA unwrapping. In line with this finding, nucleosomes containing histone variants CENP-A or H2A.B present remarkable elasticity, underscoring the importance of structural rigidity for generating specific nucleosome properties (Tachiwana et al., 2011; Zhou et al., 2021).

Swc2 recognizes the inherent instability of A-Nuc and selectively facilitates the disassembly of nucleosomes containing the H2A M4 region, underlining a central role of the H2A/H2A.Z M4 region in regulating nucleosome stability. Nonetheless, it is worth noting that other H2A residues, such as those within the α1 helix and L2 loop, might contribute to SWR1 activation and nucleosome dynamics modulation (Ranjan et al., 2015). Future studies will be necessary to elaborate on whether they modulate SWR1 activation by influencing nucleosome stability.

STAR★METHODS

Detailed methods are provided in the online version of this paper and include the following:

- KEY RESOURCES TABLE
- RESOURCE AVAILABILITY
  - Lead contact
  - Materials availability
  - Data and code availability

SUPPLEMENTAL INFORMATION

Supplemental information can be found online at https://doi.org/10.1016/j.celrep.2021.109183.

ACKNOWLEDGMENTS

We thank Drs. Carl Wu, Ed Luk, and Anand Ranjan for comments; staff at the Shanghai Synchrotron Radiation Facility for technical support of crystallographic data collection; and members of the Z. Zhou and W.L. laboratories for helpful discussions and critical comments on the manuscript. This work was supported by research grants from the Natural Science Foundation of China (31521002, 32000421, 21991133, 11874414, 31770812, 11774407, 11874415), Key Research Program on Frontier Science (QYZDB-SSW-SLH045), National Key Research and Development Program (2016YFA0301500), CAS Strategic Priority Research Program (XDB37010100), and National Laboratory of Biomacromolecules (2020kf02).

AUTHOR CONTRIBUTIONS

Z. Zhou and W.L. conceived the study. L.D., W.L., and Z. Zhou designed the experiments, analyzed the data, and wrote the manuscript. L.D. prepared proteins; performed NMR, CD, and exchange experiments; and determined the structure. X.X. performed the single-molecule magnetic tweezer experiments. L.P. and Z. Zhang performed the ChIP-seq assay. L.S. performed the EMSA assays. N.X. analyzed the NMR data. X.F., L.M., and S.D. contributed to biochemical assays and magnetic tweezer analysis.

DECLARATION OF INTERESTS

The authors declare no competing interests.

Received: January 14, 2021
Revised: March 29, 2021
Accepted: May 5, 2021
Published: May 25, 2021

REFERENCES

Abbott, D.W., Ivanova, V.S., Wang, X., Bonner, W.M., and Ausió, J. (2001). Characterization of the stability and folding of H2A.Z chromatin particles: implications for transcriptional activation. J. Biol. Chem. *276*, 41945–41949.

Adams, P.D., Grosse-Kunstleve, R.W., Hung, L.W., Ioerger, T.R., McCoy, A.J., Moriarty, N.W., Read, R.J., Sacchettini, J.C., Sauter, N.K., and Terwilliger, T.C. (2002). PHENIX: building new software for automated crystallographic structure determination. Acta Crystallogr. D Biol. Crystallogr. *58*, 1948–1954.

Armeev, G.A., Gribkova, A.K., Pospelova, I., Komarova, G.A., and Shaytan, A.K. (2019). Linking chromatin composition and structural dynamics at the nucleosome level. Curr. Opin. Struct. Biol. *56*, 46–55.

Bintu, L., Ishibashi, T., Dangkulwanich, M., Wu, Y.-Y., Lubkowska, L., Kashlev, M., and Bustamante, C. (2012). Nucleosomal elements that control the topography of the barrier to transcription. Cell *151*, 738–749.

Chen, P., Zhao, J., Wang, Y., Wang, M., Long, H., Liang, D., Huang, L., Wen, Z., Li, W., Li, X., et al. (2013). H3.3 actively marks enhancers and primes gene transcription via opening higher-ordered chromatin. Genes Dev. *27*, 2109–2124.

Chen, P., Dong, L., Hu, M., Wang, Y.-Z., Xiao, X., Zhao, Z., Yan, J., Wang, P.-Y., Reinberg, D., Li, M., et al. (2018). Functions of FACT in breaking the nucleosome and maintaining its integrity at the single-nucleosome level. Mol. Cell *71*, 284–293.e4.

Dai, L., Xu, N., and Zhou, Z. (2019). NMR investigations on H2A-H2B heterodimer dynamics conferred by histone variant H2A.Z. Biochem. Biophys. Res. Commun. *518*, 752–758.

Daldrop, P., Brutzer, H., Huhle, A., Kauert, D.J., and Seidel, R. (2015). Extending the range for force calibration in magnetic tweezers. Biophys. J. *108*, 2550–2561.

Delaglio, F., Grzesiek, S., Vuister, G.W., Zhu, G., Pfeifer, J., and Bax, A. (1995). NMRPipe: a multidimensional spectral processing system based on UNIX pipes. J. Biomol. NMR *6*, 277–293.

Dyer, P.N., Edayathumangalam, R.S., White, C.L., Bao, Y., Chakravarthy, S., Muthurajan, U.M., and Luger, K. (2004). Reconstitution of nucleosome core particles from recombinant histones and DNA. Methods Enzymol. *375*, 23–44.

Emsley, P., and Cowtan, K. (2004). Coot: model-building tools for molecular graphics. Acta Crystallogr. D Biol. Crystallogr. *60*, 2126–2132.

Gosse, C., and Croquette, V. (2002). Magnetic tweezers: micromanipulation and force measurement at the molecular level. Biophys. J. *82*, 3314–3329.

Guillemette, B., and Gaudreau, L. (2006). Reuniting the contrasting functions of H2A.Z. Biochem. Cell Biol. *84*, 528–535.

Hall, M.A., Shundrovsky, A., Bai, L., Fulbright, R.M., Lis, J.T., and Wang, M.D. (2009). High-resolution dynamic mapping of histone-DNA interactions in a nucleosome. Nat. Struct. Mol. Biol. *16*, 124–129.

Henikoff, S., and Smith, M.M. (2015). Histone variants and epigenetics. Cold Spring Harb. Perspect. Biol. *7*, a019364.

Hong, J., Feng, H., Wang, F., Ranjan, A., Chen, J., Jiang, J., Ghirlando, R., Xiao, T.S., Wu, C., and Bai, Y. (2014). The catalytic subunit of the SWR1 remodeler is a histone chaperone for the H2A.Z-H2B dimer. Mol. Cell *53*, 498–505.

Huang, Y., Dai, Y., and Zhou, Z. (2020a). Mechanistic and structural insights into histone H2A-H2B chaperone in chromatin regulation. Biochem. J. *477*, 3367–3386.

Huang, Y., Sun, L., Pierrakeas, L., Dai, L., Pan, L., Luk, E., and Zhou, Z. (2020b). Role of a DEF/Y motif in histone H2A-H2B recognition and nucleosome editing. Proc. Natl. Acad. Sci. USA *117*, 3543–3550.

Kemble, D.J., McCullough, L.L., Whitby, F.G., Formosa, T., and Hill, C.P. (2015). FACT disrupts nucleosome structure by binding H2A-H2B with conserved peptide motifs. Mol. Cell *60*, 294–306.

Kim, J., Wei, S., Lee, J., Yue, H., and Lee, T.-H. (2016). Single-molecule observation reveals spontaneous protein dynamics in the nucleosome. J. Phys. Chem. B *120*, 8925–8931.

Laskowski, R.A., MacArthur, M.W., Moss, D.S., and Thornton, J.M. (1993). PROCHECK: a program to check the stereochemical quality of protein structures. J. Appl. Crystallogr. *26*, 283–291.

Latrick, C.M., Marek, M., Ouararhni, K., Papin, C., Stoll, I., Ignatyeva, M., Obri, A., Ennifar, E., Dimitrov, S., Romier, C., and Hamiche, A. (2016). Molecular

basis and specificity of H2A.Z-H2B recognition and deposition by the histone chaperone YL1. Nat. Struct. Mol. Biol. *23*, 309–316.

Li, W., Chen, P., Yu, J., Dong, L., Liang, D., Feng, J., Yan, J., Wang, P.-Y., Li, Q., Zhang, Z., et al. (2016). FACT remodels the tetranucleosomal unit of chromatin fibers for gene transcription. Mol. Cell *64*, 120–133.

Liang, X., Shan, S., Pan, L., Zhao, J., Ranjan, A., Wang, F., Zhang, Z., Huang, Y., Feng, H., Wei, D., et al. (2016). Structural basis of H2A.Z recognition by SRCAP chromatin-remodeling subunit YL1. Nat. Struct. Mol. Biol. *23*, 317–323.

Lowary, P.T., and Widom, J. (1998). New DNA sequence rules for high affinity binding to histone octamer and sequence-directed nucleosome positioning. J. Mol. Biol. *276*, 19–42.

Luger, K., Mäder, A.W., Richmond, R.K., Sargent, D.F., and Richmond, T.J. (1997). Crystal structure of the nucleosome core particle at 2.8 Å resolution. Nature *389*, 251–260.

Luger, K., Rechsteiner, T.J., and Richmond, T.J. (1999). Expression and purification of recombinant histones and nucleosome reconstitution. Methods Mol. Biol. *119*, 1–16.

Luk, E., Ranjan, A., Fitzgerald, P.C., Mizuguchi, G., Huang, Y., Wei, D., and Wu, C. (2010). Stepwise histone replacement by SWR1 requires dual activation with histone H2A.Z and canonical nucleosome. Cell *143*, 725–736.

Mao, Z., Pan, L., Wang, W., Sun, J., Shan, S., Dong, Q., Liang, X., Dai, L., Ding, X., Chen, S., et al. (2014). Anp32e, a higher eukaryotic histone chaperone directs preferential recognition for H2A.Z. Cell Res. *24*, 389–399.

McCoy, A.J., Grosse-Kunstleve, R.W., Adams, P.D., Winn, M.D., Storoni, L.C., and Read, R.J. (2007). Phaser crystallographic software. J. Appl. Crystallogr. *40*, 658–674.

Mihardja, S., Spakowitz, A.J., Zhang, Y., and Bustamante, C. (2006). Effect of force on mononucleosomal dynamics. Proc. Natl. Acad. Sci. USA *103*, 15871–15876.

Mizuguchi, G., Shen, X., Landry, J., Wu, W.H., Sen, S., and Wu, C. (2004). ATP-driven exchange of histone H2AZ variant catalyzed by SWR1 chromatin remodeling complex. Science *303*, 343–348.

Obri, A., Ouararhni, K., Papin, C., Diebold, M.-L., Padmanabhan, K., Marek, M., Stoll, I., Roy, L., Reilly, P.T., Mak, T.W., et al. (2014). ANP32E is a histone chaperone that removes H2A.Z from chromatin. Nature *505*, 648–653.

Osakabe, A., Lorkovic, Z.J., Kobayashi, W., Tachiwana, H., Yelagandula, R., Kurumizaka, H., and Berger, F. (2018). Histone H2A variants confer specific properties to nucleosomes and impact on chromatin accessibility. Nucleic Acids Res. *46*, 7675–7685.

Otwinowski, Z., and Minor, W. (1997). Processing of X-ray diffraction data collected in oscillation mode. Methods Enzymol. *276*, 307–326.

Park, Y.-J., Dyer, P.N., Tremethick, D.J., and Luger, K. (2004). A new fluorescence resonance energy transfer approach demonstrates that the histone variant H2AZ stabilizes the histone octamer within the nucleosome. J. Biol. Chem. *279*, 24274–24282.

Ranjan, A., Mizuguchi, G., FitzGerald, P.C., Wei, D., Wang, F., Huang, Y., Luk, E., Woodcock, C.L., and Wu, C. (2013). Nucleosome-free region dominates histone acetylation in targeting SWR1 to promoters for H2A.Z replacement. Cell *154*, 1232–1245.

Ranjan, A., Wang, F., Mizuguchi, G., Wei, D., Huang, Y., and Wu, C. (2015). H2A histone-fold and DNA elements in nucleosome activate SWR1-mediated H2A.Z replacement in budding yeast. eLife *4*, e06845.

Rudnizky, S., Bavly, A., Malik, O., Pnueli, L., Melamed, P., and Kaplan, A. (2016). H2A.Z controls the stability and mobility of nucleosomes to regulate expression of the LH genes. Nat. Commun. *7*, 12958.

Smith, S.B., Finzi, L., and Bustamante, C. (1992). Direct mechanical measurements of the elasticity of single DNA molecules by using magnetic beads. Science *258*, 1122–1126.

Sun, L., Pierrakeas, L., Li, T., and Luk, E. (2020). Thermosensitive nucleosome editing reveals the role of DNA sequence in targeted histone variant deposition. Cell Rep. *30*, 257–268.e5.

Suto, R.K., Clarkson, M.J., Tremethick, D.J., and Luger, K. (2000). Crystal structure of a nucleosome core particle containing the variant histone H2A.Z. Nat. Struct. Biol. *7*, 1121–1124.

Tachiwana, H., Kagawa, W., Shiga, T., Osakabe, A., Miya, Y., Saito, K., Hayashi-Takanaka, Y., Oda, T., Sato, M., Park, S.-Y., et al. (2011). Crystal structure of the human centromeric nucleosome containing CENP-A. Nature *476*, 232–235.

Thambirajah, A.A., Dryhurst, D., Ishibashi, T., Li, A., Maffey, A.H., and Ausió, J. (2006). H2A.Z stabilizes chromatin in a way that is dependent on core histone acetylation. J. Biol. Chem. *281*, 20036–20044.

Tsunaka, Y., Kajimura, N., Tate, S., and Morikawa, K. (2005). Alteration of the nucleosomal DNA path in the crystal structure of a human nucleosome core particle. Nucleic Acids Res. *33*, 3424–3434.

Venkatesh, S., and Workman, J.L. (2015). Histone exchange, chromatin structure and the regulation of transcription. Nat. Rev. Mol. Cell Biol. *16*, 178–189.

Wang, Y., Liu, S., Sun, L., Xu, N., Shan, S., Wu, F., Liang, X., Huang, Y., Luk, E., Wu, C., and Zhou, Z. (2019). Structural insights into histone chaperone Chz1-mediated H2A.Z recognition and histone replacement. PLoS Biol. *17*, e3000277.

Watanabe, S., Radman-Livaja, M., Rando, O.J., and Peterson, C.L. (2013). A histone acetylation switch regulates H2A.Z deposition by the SWR-C remodeling enzyme. Science *340*, 195–199.

Willhoft, O., Ghoneim, M., Lin, C.-L., Chua, E.Y.D., Wilkinson, M., Chaban, Y., Ayala, R., McCormack, E.A., Ocloo, L., Rueda, D.S., and Wigley, D.B. (2018). Structure and dynamics of the yeast SWR1-nucleosome complex. Science *362*, eaat7716.

Wu, W.-H., Alami, S., Luk, E., Wu, C.-H., Sen, S., Mizuguchi, G., Wei, D., and Wu, C. (2005). Swc2 is a widely conserved H2AZ-binding module essential for ATP-dependent histone exchange. Nat. Struct. Mol. Biol. *12*, 1064–1071.

Wu, W.-H., Wu, C.-H., Ladurner, A., Mizuguchi, G., Wei, D., Xiao, H., Luk, E., Ranjan, A., and Wu, C. (2009). N terminus of Swr1 binds to histone H2AZ and provides a platform for subunit assembly in the chromatin remodeling complex. J. Biol. Chem. *284*, 6200–6207.

Yen, K., Vinayachandran, V., and Pugh, B.F. (2013). SWR-C and INO80 chromatin remodelers recognize nucleosome-free regions near +1 nucleosomes. Cell *154*, 1246–1256.

Zhou, M., Dai, L., Li, C., Shi, L., Huang, Y., Guo, Z., Wu, F., Zhu, P., and Zhou, Z. (2021). Structural basis of nucleosome dynamics modulation by histone variants H2A.B and H2A.Z.2.2. EMBO J. *40*, e105907.

Zlatanova, J., and Thakar, A. (2008). H2A.Z: view from the top. Structure *16*, 166–179.

STAR★METHODS

KEY RESOURCES TABLE

REAGENT or RESOURCE	SOURCE	IDENTIFIER
Antibodies		
Polyclonal anti-Htz1	Abcam	Cat# ab4626; RRID: AB_449326
Bacterial and virus strains		
E. coli strain BL21 CodonPLUS(DE3)-RIPL	Agilent	Cat# 230280
Chemicals, peptides, and recombinant proteins		
TSKgel DEAE-5PW column	TOSOH	Cat# 0007574
Ni-NTA resin	QIAGEN	Cat# 30230
Hitrap Q HP	GE healthcare	Cat# 17-1154-01
Hitrap SP HP	GE healthcare	Cat# 17-1151-01
Superdex 200 10/300 GL	GE Healthcare	Cat# 17-5175-01
Dynabeads Protein A	Thermo Fisher	Cat# 10001D
Glass beads, acid-washed	Sigma-Aldrich	Cat# G8772-500G
Amylose Resin High Flow	NEB	Cat# E8022s
Anti-Flag Affinity Resin	Thermo Fisher	Cat# A36803
Phenylmethylsulfonyl fluoride (PMSF)	Millipore Sigma	Cat# 11359061001
Pepstatin A	Amresco	Cat# J583
Chymostatin	Sigma-Aldrich	Cat# C7258
Leupeptin	Millipore Sigma	Cat# 62070-10MG-F
Benzamidine hydrochloride	Millipore Sigma	Cat# B6506-100G
Lambda Phage DNA	NEB	Cat# N3011L
3xFlag peptide	SciLight	Cat# C233111
Experimental models: organisms/strains		
W1588-4C *SWR1-3xFLAG-loxP RVB1-MBP-loxP htz1Δ::kanMX*	Ed Luk	N/A
W1588-4C *SWR1-3xFLAG-loxP RVB1-MBP-loxP htz1Δ::kanMX SWC2Δ*	Ed Luk	N/A
W1588-4C *SWR1-3xFLAG kanMX4 SWC2::hphMX6*	Wu et al., 2005	N/A
Oligonucleotides		
409 DNA F primer: 5′-(biotin) GGAAACAGCTATGACCATG	Sangon Biotech	N/A
409 DNA R primer: 5′-(digoxin) GTAAAACGACGGCCAGTGAGCG	Sangon Biotech	N/A
204 DNA F primer: TCTTCACAC CGAGTTCATCCCTT	Sangon Biotech	N/A
204 DNA R primer: TACATGCACAGGATGTATATATCTGAC	Sangon Biotech	N/A
147 DNA F primer: 5′-(Cy3) CTGG AGAATCCCGGTG	Sangon Biotech	N/A
147 DNA R primer: TCCAGTGCCGGTGTCG	Sangon Biotech	N/A
Deposited data		
Coordinates of $H2A^{M4>Z}$-H2B	This Paper	PDB: 7DLX
Coordinates of H2A-H2B	Kemble et al., 2015	PDB: 4WNN
Coordinates of dYL-H2A.Z-H2B	Liang et al., 2016	PDB: 5CHL

(*Continued on next page*)

Continued

REAGENT or RESOURCE	SOURCE	IDENTIFIER
Coordinates of the human nucleosome	Tsunaka et al., 2005	PDB: 2CV5
ChIP-seq Data	This Paper	GEO: GSE171844
Recombinant DNA		
pET-28a Swc2-Z (1-135)	This Paper	N/A
pET-28a Swc2-ZN	This Paper	N/A
pET-28a Swc2-ZC	This Paper	N/A
pET-28a Swc2-$Z^{3R/A}$	This Paper	N/A
pET-28a hYL1-Z (1-77)	This Paper	N/A
pET-3a yH2A	This Paper	N/A
pET-3a $yH2A^{M4>Z}$	This Paper	N/A
pET-3a $yH2A^{M6>Z}$	This Paper	N/A
pET-3a yH2A.Z	This Paper	N/A
pET-3a $yH2A.Z^{M4>A}$	This Paper	N/A
pET-3a $yH2A.Z^{M6>A}$	This Paper	N/A
pET-3a yH2B	This Paper	N/A
pET-17b-$H2A^{M4>Z}$-H2B	This Paper	N/A
pET-3a $yH2A.Z^{FLAG}$	This Paper	N/A
pET-3a flyH3	This Paper	N/A
pET-3a flyH4	This Paper	N/A
pET-3a xlH2A	Luger et al., 1999	N/A
pET-3a xlH2B	Luger et al., 1999	N/A
pET-3a xlH3	Luger et al., 1999	N/A
pET-3a xlH4	Luger et al., 1999	N/A
pRS416-Swc2-ΔZ	This Paper	N/A
pRS416-Swc2-ΔZN	This Paper	N/A
pRS416-Swc2-3R/A	This Paper	N/A
Software and algorithms		
Pymol	Schrödinger LLC	http://www.pymol.org
Graphpad Prism8	GraphPad software	https://www.graphpad.com
NMRViewJ	One Moon Scientific, Inc.	https://nmrfx.org/nmrfx/nmrviewj
NMRPipe	Delaglio et al., 1995	https://www.ibbr.umd.edu/nmrpipe/index.html
Sparky	T. D. Goddard and D. G. Kneller, SPARKY 3, University of California, San Francisco	https://www.cgl.ucsf.edu/home/sparky/
COOT	Emsley and Cowtan, 2004	https://www2.mrc-lmb.cam.ac.uk/personal/pemsley/coot/
Phenix	Adams et al., 2002	https://www.phenix-online.org/
Quantity One	BioRad	https://www.bio-rad.com/zh-cn/SearchResults?Text=Quantity+One

RESOURCE AVAILABILITY

Lead contact

Further information and requests for resources and reagents should be directed to and will be fulfilled by the Lead Contact, Zheng Zhou (zhouzh@ibp.ac.cn).

Materials availability

Plasmids generated in this study will be made available on request, but we may require a payment and/or a completed Materials Transfer Agreement if there is potential for commercial application.

Data and code availability

The atomic coordinates and structure factors have been deposited in the Protein Data bank (http://www.rcsb.org) with PDB: 7DLX. The accession number for the ChIP-seq data reported in this paper is GEO: GSE171844. All deposited data will be available upon publication of the study.

EXPERIMENTAL MODEL AND SUBJECT DETAILS

Bacterial strains

Swc2 and hYL1 genes were isolated from *Saccharomyces cerevisiae* and *Homo sapiens*, respectively. *E.coli* strain BL21 Codon PLUS(DE3)-RIPL (Agilent) was used for protein expression. Cells were grown in standard LB media at 37°C.

Yeast strains

Saccharomyces cerevisiae strains W1588-4C-htz1Δ (W1588-4C *SWR1-3xFLAG-loxP RVB1-MBP-loxP htz1Δ::kanMX*), W1588-4C-htz1ΔSWC2Δ (W1588-4C *SWR1-3xFLAG-loxP RVB1-MBP-loxP htz1Δ::kanMX SWC2Δ*) and W1588-4C-SWC2Δ (W1588-4C *SWR1-3xFLAG kanMX4 SWC2::hphMX6*) were used for purification of SWR1 complex. The strains harboring wide-type Swc2 gene were grown in YPD media, supplemented with adenine, at 30°C until an OD_{600} of ~4. The *SWC2Δ* strains harboring pRS416 plasmids were grown in CSM-URA media.

METHOD DETAILS

Cloning, expression, and purification of recombinant proteins

Various regions of Swc2 (hYL1) gene were amplified from the plasmid containing the coding sequence of Swc2 (hYL1) and cloned into pET28a vectors. Mutations were made using the Quikhange kit. *E.Coli* BL21-CodonPlus(DE3)-RIPL was used for the expression of Swc2, hYL1 and histone proteins. Expression of the His-tagged Swc2 and hYL1 proteins was induced by the addition of 0.5 mM IPTG for 20-24 h at 16°C. Cells were lysed by sonication in buffer A (20 mM Tris-HCl pH 8.0, 8 M Urea, 20 mM imidazole). Clarified lysate was applied to a column of Ni-NTA resin (QIAGEN). After extensive washing in buffer A, the protein was eluted with buffer B (20 mM Tris-HCl pH 8.0, 8 M Urea, 250 mM imidazole), further purified over HiTrap Q anion-exchange column (GE Healthcare) equilibrated with buffer C (20 mM Tris-HCl pH 8.0, 8 M Urea) using an ÄKTA FPLC system (GE Healthcare). The target protein containing peak was collected and dialyzed against buffer D (20 mM Tris-HCl pH 8.0, 150 mM NaCl), followed by digestion with Thrombin (Fisher Scientific) protease. The protein was concentrated and further purified on Superdex-200 gel-filtration column (GE Healthcare) in buffer D. Protein-containing fractions were concentrated and stored at −80°C. Isotope-labeled proteins for NMR studies were expressed by growing *E. coli* cells in M9 media with ^{15}N labeled NH_4Cl, U-$^{13}C6$-Glucose, as the sole source for nitrogen, carbon, respectively.

E.Coli were transformed with histone expression plasmids and grown in 2xYT medium at 37°C to OD_{600} of ~0.6. Protein expression was induced by the addition of 0.5 mM IPTG for 2-3 h at 37°C. Cell pellets were resuspended and lysed by sonication in buffer D (20 mM Tris-HCl pH 8.0, 150 mM NaCl). Inclusion bodied were isolated by centrifugation at 30,000 g for 1 h at 4°C and washed twice with buffer D containing 1% (w/v) Triton X-100. Inclusion bodies were washed one final time with buffer D and centrifuged at 30,000 g for 15 min at 4°C. Inclusion bodies were resuspended in a guanidine hydrochloride denaturing buffer E (20 mM Tris-Cl pH 8.0, 7 M guanidine-HCl), followed by centrifugation at 80,000 g for 30 min at 4°C. The supernatant was dialyzed against buffer C (20 mM Tris-HCl pH 8.0, 8 M Urea), and further purified over HiTrap SP cation-exchange column (GE Healthcare). Protein-containing fractions were collected and stored at 4°C

To obtain H2A-H2B dimer, purified H2A and H2B were mixed at 1:1 stoichiometry and dialyzed against buffer F (20 mM Tris-HCl pH 8.0, 0.5 M NaCl). The refolded histone dimer was loaded onto a HiTrap SP cation-exchange chromatography (GE Healthcare) and eluted using a gradient of salt. Similarly, purified H3 and H4 were mixed at 1:1 stoichiometry and dialyzed against 2TEN buffer (10 mM Tris-HCl, pH 7.5, 1 mM EDTA, 2 M NaCl). The refolded H3-H4 tetramer was further purified on Superdex-200 gel-filtration column (GE Healthcare) in 2TEN buffer. Protein-containing fractions were collected and stored at −80°C. The expression and purification of protein mutants and variants were identical to those of their wide-type proteins.

Preparation of DNAs

Large-scale quantities of 147-bp Widom 601 DNA for NMR assay was purified as described previously from the pUC19 12x147 bp 601-sequence using *Eco*RV restriction enzyme to digest the DNA into fragments (Luger et al., 1999; Zhou et al., 2021). DNA fragments for magnetic tweezers' investigation were generated by PCR, essentially as described previously (Chen et al., 2018). The 409-bp DNA containing a single 601 sequence were prepared by PCR from plasmid using a biotin (bio)-labeled forward primer [5′-(biotin) GGAAACAGCTATGACCATG] and a digoxigenin (dig)-labeled reverse primer [5′-(digoxin) GTAAAACGACGGCCAGTGAGCG]. The products were pooled from two 48-well PCR plates (50 μL per well). The PCR products were applied to a HiTrap Q column (GE Healthcare) and eluted with a gradient from 0%–100% TE high salt buffer (10 mM Tris pH 7.5, 1 M NaCl, 1 mM EDTA). Peak fractions were analyzed on a 5% (v/v) native-page gel and fractions containing the desired DNA product were pooled. The products were ethanol-precipitated, resuspended in 500 μL TE buffer (10 mM Tris pH 7.5,1 mM EDTA), and stored at −20°C. DNA fragments used to generate the 204-bp (50-N-7) nucleosome were prepared by PCR from plasmid using two primers (forward: TCTTCACACCGAGTTCATCCCTT, reverse:

TACATGCACAGGATGTATATATCTGAC), essentially as described previously (Sun et al., 2020). The amplification and purification of 204-bp DNA were identical to those of 409-bp DNA. For EMSA assay, the Cy3-labeled 147-DNA were prepared by PCR form 147-DNA fragment using a Cy3-labeled forward primer [5′-(Cy3) CTGGAGAATCCCGGTG]. The PCR products were purified using 1% (v/v) TAE agarose gel and gel extraction kit (TIANGEN). All DNA concentrations were determined via absorbance at 260 nm using a NANODROP 2000c (Thermo Scientific) and stored at −20°C.

Nucleosome reconstitution

Nucleosome reconstitution was performed as previously described (Dyer et al., 2004), with minor modifications. Briefly, histone octamers were reconstituted by mixing the purified H2A-H2B dimers and H3-H4 tetramers at equimolar ratio in 2TEN buffer. Correctly folded octamers were further purified using Superdex-200 gel-filtration column (GE Healthcare) in 2TEN buffer. Histone octamer and DNA were mixed at a 1:1 molar ratio in 2TEN buffer. The sample was gradient dialyzed for 20 h at 4°C, which was continuously diluted by slowly pumping in TE buffer (10 mM Tris-HCl, pH 7.5, 1 mM EDTA) to a lower concentration of NaCl from 2 M to 0.4 M. The sample was collected after final dialysis in TE buffer for 4 h. Note that the 147-nucleosome for NMR assay was further incubated at 55°C for 2 h, then purified from the free DNA using DEAE-5PW column (TOSOH). The nucleosome-containing fractions were pooled and dialyzed against TE buffer. All nucleosome concentrations were determined via absorbance at 260 nm using a NANODROP 2000c (Thermo Scientific), followed by native-PAGE and ethidium bromide staining with comparison to known amounts of control DNA fragments. The reconstitution of nucleosomes containing histone mutants was identical to those of their wide type.

NMR experiments

NMR experiments were performed on a Varian 600-MHz spectrometer. Experiments of 2D ^{1}H-^{15}N HSQC, 3D CBCANH, CBCA(CO)NH, HNCA, HN(CO)CA were performed. NMRPipe (Delaglio et al., 1995) and Sparky (http://www.cgl.ucsf.edu/home/sparky/) were used to process the spectra.

AFM analysis

Glutaraldehyde was diluted in HE buffer (10 mM HEPES-NaOH pH7.6, 1 mM EDTA) to a concentration of 0.2%. 5 μL nucleosome sample was mixed with 5 μL 0.2% glutaraldehyde on ice for 30 min. The mixture was spun at a speed of 15,000 g in a vivaspin 500 column for 2-5 min at 4°C to get rid of the redundant glutaraldehyde. Then the sample was diluted in HE buffer with a concentration of 0.5 ng/μL. The fresh mica surface was incubated with 1 mM spermidine for 10 min, rinsed with 1 mL ddH_2O and dried gently with nitrogen gas. The prepared sample was incubated to the mica surface for 10 min. The mica was rinsed with 1 mL ddH_2O and dried. Then the mica was scanned using ScanAsyst Mode of AFM (MultiMode 8 SPM system, BRUKER).

Single-molecule magnetic tweezers data analysis

The nucleosome sample was tethered between a super-paramagnetic bead and a coverslip in the flow cell. Above the flow cell, the permanent magnets can exert force on the super-paramagnetic bead, therefore exerting forces on the nucleosome samples. Below the flow cell, the objective and the CCD camera can record diffraction patterns of the beads in experiments.

The range of exerted force of the permanent magnet is 0∼100 pN, which is controlled by regulating the distance of magnets in z direction. To calibrate the force, a 10 kb DNA fragment was stretched at each magnetic position. The lateral position of super-paramagnetic beads was recorded for 5 min and the corresponding force was calibrated by PSD analysis (Daldrop et al., 2015). The relation between the magnets' position and the corresponding force was fitted by exponential function (Gosse and Croquette, 2002).

To acquire the position of the magnetic beads in z direction, a look-up table (LUT) of the diffraction pattern of the beads was established by recording the diffraction pattern when the objective is moving at a ∼100 nm step size, with the magnets exerting 2∼3 pN to the beads to reduce the fluctuation of beads. Then by interpolating, the precise z value can be compared and calculated by the LUT.

Force-extension measurement of mono-nucleosome

A flow cell consists of a bottom functionalized coverslip, a double-sided tape with a rectangular channel (5x50 mm^2), and an upper coverslip with two holes at each end to be used as inlet and outlet. The bottom coverslip was coated with polystyrene beads to offset the thermal drift. The flow cell was first incubated with anti-digoxigenin (0.1 mg/mL) for at least 2 h and then passivated with 10 mg/mL BSA for at least 8 h. Nucleosome samples labeled with digoxigenin and biotin at each end of DNA were then injected into the flow cell and tethered between the super-paramagnetic bead (M280 Invitrogen Norway) and the coverslip (Smith et al., 1992). Afterward, Swc2 protein was injected into the flow cell and incubated for 30 min. To trace the detail of the structural transition of nucleosome samples, we used the force-ramp mode. The force exerted on the nucleosomes increased at a rate of 0.05 pN/s from 0 pN to 40 pN. For canonical nucleosomes, the rupture force of the outer wrap is ∼5 pN and that of the inner wrap is ∼23 pN, with the force increasing. The force-extension curves and statistical measurements were processed using labview software and MATLAB.

Crystallization, diffraction data collection, and structure determination

The expression and purification of single-chain yeast H2B-H2A$^{M4>Z}$ were performed as described previously (Dai et al., 2019). Briefly, *E.Coli* were transformed with yeast H2B-H2A$^{M4>Z}$ expression plasmids (pET17b, Novagen) and grown in LB medium at 37°C to

OD_{600} of ~1.0. Protein expression was induced by the addition of 0.5 mM IPTG for 5 h at 37°C. Cell pellets were resuspended and lysed by sonication in buffer F (20 mM Tris-HCl pH 8.0, 0.5 M NaCl). Clarified lysate was applied to SP Sepharose fast flow beads (GE Healthcare). After extensive washing in buffer F, the protein was eluted with buffer G (20 mM Tris-HCl pH 8.0, 1 M NaCl), further purified over HiTrap SP cation-exchange column (GE Healthcare) equilibrated with lysis buffer using an ÄKTA FPLC system (GE Healthcare). Protein-containing fractions were collected, dialyzed against buffer H (20 mM MES pH 6.0, 0.2 M NaCl) and concentrated for crystallization. Crystals were grown at 16°C from hanging drops composed of 1 μL of protein solution (10 mg/ml) and 1 μL of crystallization buffer (0.1 M BIS-TRIS propane pH 7.0, 4 M Sodium nitrate) suspended over 0.2 mL of the latter. The crystals were flash frozen in liquid nitrogen with 20% glycerol as cryoprotectant. X-ray diffraction data was collected at Shanghai Synchrotron Radiation Facility (SSRF) on beamline BL17U with a Quantum 315r CCD detector (ADSC). Data were processed, integrated, and scaled with the HKL2000 package (Otwinowski and Minor, 1997). The structure was solved using the PDB: 5CHL (Chain B) as a search model by molecular replacement (PHASER) (McCoy et al., 2007). Manual model building and refinement were performed with COOT (Emsley and Cowtan, 2004) and PHENIX (Adams et al., 2002). During the later stages of positional refinement, restraints were relaxed, and bulk solvent correction was applied under the guidance of R_{free} Model geometry was verified with PROCHECK (Laskowski et al., 1993). The data and refinement statistics are summarized in Table S1.

Thermal stability assay

The thermal stability assay was conducted in 400 μL of 20 mM MES (pH6.0) buffer containing 0.5 M NaCl. The Chirascan Plus was used to detect the CD signals with a temperature gradient from 25 to 90°C, in steps of 1°C/min.

EMSAs of DNA binding of the histone dimers

Purified histone dimers and the 147-bp Widom 601 DNA labeled with Cy3 were mixed and incubated at room temperature for 30 min. Ten percent sucrose was added for loading. Free and histone-bound DNA were resolved on 6% native-page gels. All gels were run in 0.5xTBE at 4°C. Quantification of EMSA assay was performed with Quantity One (Bio-Rad).

Histone exchange assay

The yeast strains used in this study was a gift from Ed Luk. The native ASAP-SWR1 complex were purified as described previously (Sun et al., 2020). pRS416 plasmid containing mutants Swc2-ΔZN and Swc2-3R/A were introduced into *SWC2Δ* strain (W1588-4C *SWR1-3xFLAG-loxP RVB1-MBP-loxP htz1Δ::kanMX SWC2Δ*), respectively. Purification of mutant SWR1 complex was identical to those of their wide type. *In Vitro* histone exchange reactions were performed as previously described with minor modifications (Sun et al., 2020). 5 nM nucleosomes, 2 nM ASAP-SWR1 complex, 50 nM H2A.Z-3xFlagH2A.Z-H2B dimer and 2 mM ATP were dissolved into exchange buffer [25 mM HEPES-KOH, pH 7.6, 0.37 mM EDTA, 0.35 mM EGTA, 10% glycerol, 0.017% NP-40, 1 mM DTT, 70 mM KCl, 3.6 mM $MgCl_2$, 100 μg/mL BSA and protease inhibitors (0.34 mg/mL PMSF, 0.66 mg/mL benzamidine hydrochloride, 2.74 mg/mL pepstatin A, 0.56 mg/mL leupeptin, and 4 mg/mL chymostatin)] and used in 10 μL reaction mixes. After incubation under the indicated conditions, 2.3 ng/mL of lambda phage DNA (New England Biolabs) was added to quench the reaction. The reaction mixes were directly loaded on 6% native-PAGE gels run in 0.5xTBE, followed by SYBR Green staining. SYBR Green was directly detected in gels with a Typhoon 7000 (GE Healthcare).

ChIP-seq analysis

pRS416 plasmid containing mutants Swc2-ΔZN and Swc2-ΔZ were introduced into *SWC2Δ* strain (W1588-4C *SWR1-3xFLAG kanMX4 SWC2::hphMX6*) (Wu et al., 2005), respectively. Yeast cells were fixed with 1% formaldehyde for 30 min at room temperature, followed by quenching fixation with 0.125 M glycine for 5 min. Cell wall was disrupted using Ziconia beads and lysed in lysis buffer (50 mM Tris pH7.5, 1mM EDTA pH8.0, 1% Triton X-100, 150 mM NaCl, 1xprotease inhibitors). Chromatin was sonicated to an average length of approximately 250 bp. The lysates were clarified by centrifugation, and the supernatants were incubated with protein A/G beads overnight at 4°C to remove non-specific binding. Supernatant were collected by centrifugation and added anti-Htz1 antibody (ab4626) for incubation 4 h. The Antibody-Chromatin complex were pulled down with protein A Dynabeads and were washed twice with TBST buffer, twice with TE buffer, followed by incubation with TES buffer (50 mM Tris pH7.5, 10 mM EDTA pH8.0, 1% SDS) to elute the complexes. Following cross-link reversal, Rnase A and Proteinase K treatment, phenol-chloroform extraction and ethanol precipitation, the DNA samples were used to prepared libraries with Kapa hyper prep kit and NEB Next multiples oligos for Illumina (NEB E7335) according to the operation instructions.

ChIP-seq data for H2A.Z in various *Saccharomyces cerevisiae* strains, including Swc2 WT, Swc2-ΔZ and Swc2-ΔZN, were filtered by Trim Galore and aligned to yeast genome (sacCer3) using Bowtie2 software (v2.3.5.1). Duplicates reads were discarded to remove potential PCR bias, and uniquely mapped reads were used for the subsequent analysis. Annotated genes and open reading frames (ORFs) of *S. cerevisiae* were obtained from the UCSC genome browser database (sgdGene, sacCer3). All ChIP samples were normalized to the same depth of 1 million unique mapped reads. ChIP-seq profiles around transcription start sites (TSS) were drawn using 'plotProfile' tool in deepTools (v3.4.2). Gene track profiles were visualized using IGV (v2.7.2).

QUANTIFICATION AND STATISTICAL ANALYSIS

The force-extension curves and statistical measurements were processed using labview software and MATLAB. The statistical rupture forces are illustrated in the box-and-whisker plots. The key values are called a five-number summary, which consists of the minimum, first quartile, median, third quartile, and maximum. n represents the number of data values. Center lines show the median, box limits indicate the 1^{st} and 3^{rd} quartiles. Quantifications of EMSA assay and exchange assay were performed with Quantity One (Bio-Rad) and were illustrated in Prism 8 (GraphPad).

Cell Reports, Volume *35*

Supplemental information

Recognition of the inherently unstable H2A nucleosome by Swc2 is a major determinant for unidirectional H2A.Z exchange

Linchang Dai, Xue Xiao, Lu Pan, Liuxin Shi, Ning Xu, Zhuqiang Zhang, Xiaoli Feng, Lu Ma, Shuoxing Dou, Pengye Wang, Bing Zhu, Wei Li, and Zheng Zhou

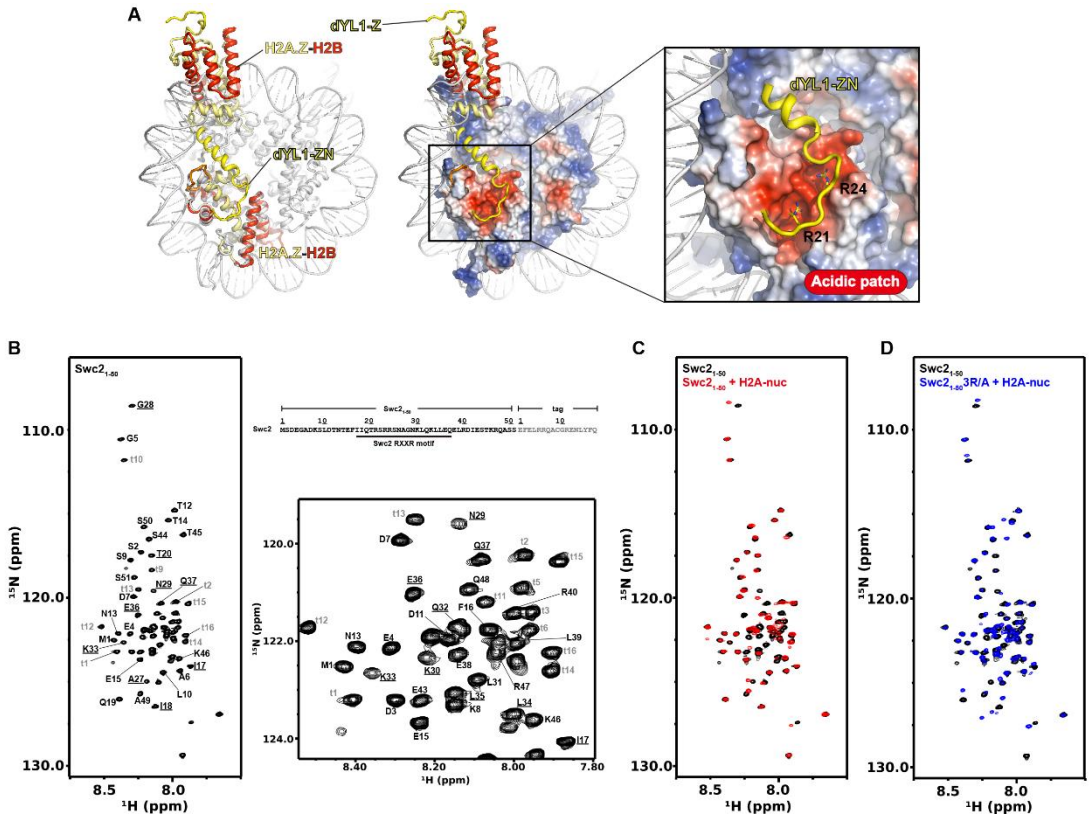

Figure S1, related to Figure 1. Swc2-ZN/YL1-ZN directly interacts with nucleosome. (A) Superimposition of Z-B dimer in the complex with dYL1-Z (PDB: 5CHL) and nucleosomal A-B dimer (PDB: 2CV5). The dYL1 residues R5 and R8 (corresponding to Swc2 R21 and R24) interacting with the histone dimer acidic region are highlighted for clear view. **(B)** NMR HSQC spectrum (left, bottom) and sequence (top) of Swc2-ZN sample. Swc2 residues 17-35 involved in H2A-nucleosome interaction are underlined in black color. Residues in the C-terminal tag of Swc2$_{1-50}$ are labelled as t1-t17 in grey colour. **(C)** Overlay of the HSQC spectra of Swc2-ZN in nucleosome-free form (black) and in nucleosome-bound form (red). **(D)** Overlay of the HSQC spectra of Swc2-ZN in nucleosome-free form (black) and Swc2-ZN containing R21A/R23A/R24A mutation (Swc2-ZN$^{3R/A}$) in nucleosome-bound form (blue).

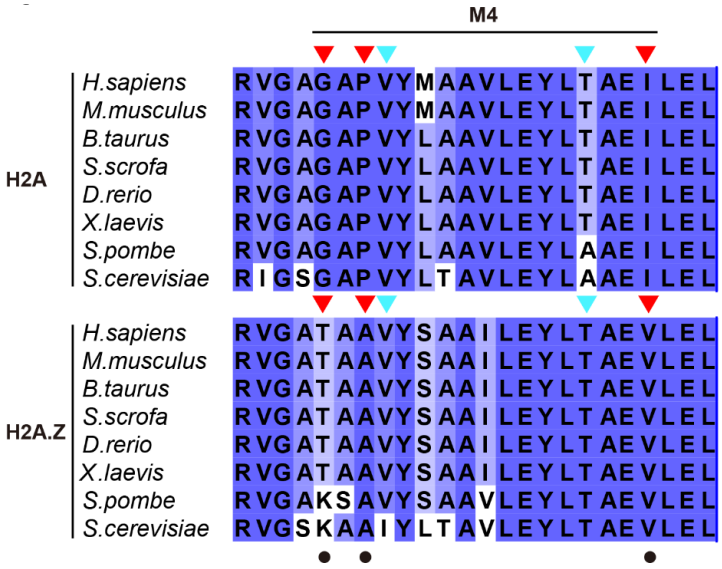

Figure S2, related to Figures 3 and 4. Multiple sequence alignment of H2A and H2A.Z M4 regions. All five yeast H2A residues discriminated from their H2A.Z counterparts are highlighted by triangles on top of the sequences. Triangles in red color highlight H2A-specific residues that show sequence conservation across all species. Triangles in blue color highlight H2A-specific residues whose sequence divergence are restricted in lower eukaryotes.

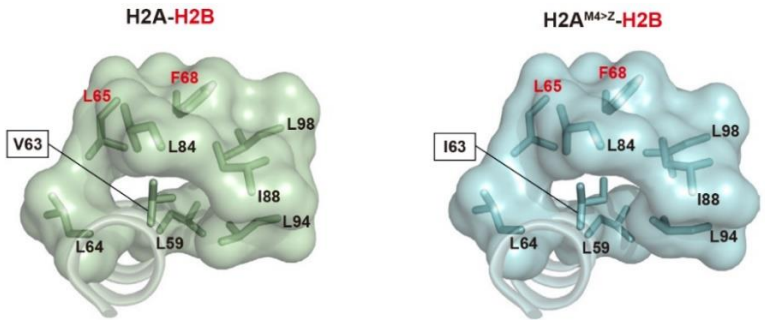

Figure S3, related to Figure 4. Structural comparison of H2A I63 in A-B dimer and H2A.Z V63 in A$^{M4>Z}$-B dimer. H2A I63 (or H2A$^{M4>Z}$ V63) and the hydrophobic residues surrounding these two residues are shown in surface mode. Histone H2A and H2A$^{M4>Z}$ residues are colored in green and cyan, respectively. The H2B residues are colored in red.

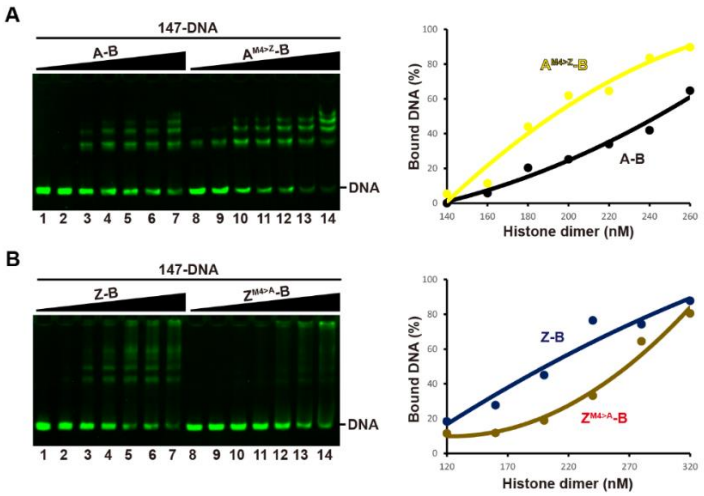

Figure S4, related to Figures 3 and 4. H2A M4 region residues reduce the binding between histone dimer and DNA. (A) EMSA showing A-B dimer or $A^{M4>Z}$-B dimer binding to DNA. Right panel shows binding carves. **(B)** EMSA showing Z-B dimer or $Z^{M4>A}$-B dimer binding to DNA. Right panel shows binding carves.

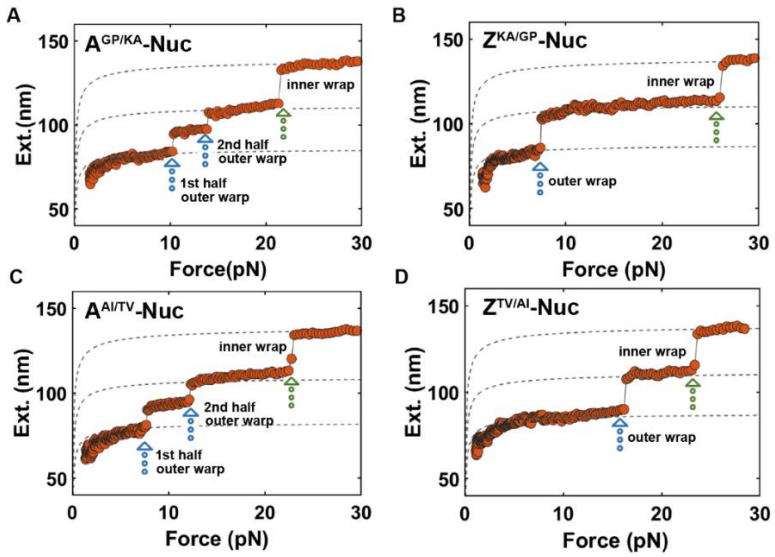

Figure S5, related to Figure 4. Typical force-extension curves of nucleosomes containing H2A$^{GP/KA}$, H2A.Z$^{KA/GP}$, H2A$^{AI/TV}$, and H2A.Z$^{TV/AI}$ mutations.

Table S1, related to Figure 4. Data collection and refinement statistics.

	$H2A^{M4>Z}$-H2B
Data collection	
Space group	P 1 21 1
Cell dimensions	
a, *b*, *c* (Å)	102.58, 73.24, 109.68
α, β, γ (°)	90.00, 95.48, 90.00
Resolution (Å)	50.00-2.40 (2.48-2.40)
R_{merge}	0.046 (0.658)
$I / \sigma I$	22.8 (2.1)
Completeness (%)	85.5 (99.8)
Redundancy	3.3 (3.6)
Refinement	
Resolution (Å)	43.77-2.40 (2.48-2.40)
No. reflections	48,153
R_{work} / R_{free}	0.23 / 0.28
No. atoms	
Protein	10,823
Water	105
B factors	
Protein	52.10
Water	37.61
r.m.s. deviations	
Bond lengths (Å)	0.002
Bond angles (°)	0.504